# Pro-tumor Tfh2 cells induce detrimental IgG4 production and $PGE_2$-dependent IgE inhibition in pancreatic cancer

Lucia De Monte,[a,b,j] Francesca Clemente,[a,b,j] Eliana Ruggiero,[b,c] Raffaella Pini,[d] Maria Grazia Ceraolo,[a,b] Marco Schiavo Lena,[e] Chiara Balestrieri,[b,c,d] Dejan Lazarevic,[d] Giulio Belfiori,[f,g] Stefano Crippa,[f,g,h] Gianpaolo Balzano,[f,g] Massimo Falconi,[f,g,h] Claudio Doglioni,[e,g,h] Chiara Bonini,[b,c,h] Michele Reni,[h,i] and Maria Pia Protti[a,b,*]

[a]Tumor Immunology Unit, Istituto di Ricovero e Cura a Carattere Scientifico (IRCCS) San Raffaele Scientific Institute, Milan, Italy
[b]Division of Immunology, Transplantation and Infectious Diseases, IRCCS San Raffaele Scientific Institute, Milan, Italy
[c]Experimental Hematology Unit, Division of Immunology, Transplantation and Infectious Diseases, IRCCS San Raffaele Scientific Institute, Milan, Italy
[d]Center for Omics Sciences, IRCCS San Raffaele Scientific Institute, Milan, Italy
[e]Pathology Unit, IRCCS San Raffaele Scientific Institute, Milan, Italy
[f]Pancreatic Surgery Unit and Pancreas Translational & Clinical Research Center, IRCCS San Raffaele Scientific Institute, Milan, Italy
[g]Division of Experimental Oncology, IRCCS San Raffaele Scientific Institute, Milan, Italy
[h]Vita-Salute San Raffaele University, Milan, Italy
[i]Department of Medical Oncology, IRCCS San Raffaele Scientific Institute, Milan, Italy

eBioMedicine
2023;97: 104819
Published Online 28 September 2023
https://doi.org/10.1016/j.ebiom.2023.104819

## Summary

**Background** Pancreatic ductal adenocarcinoma (PDAC) has a dismal prognosis and it is characterized by predominant pro-tumor Th2-type inflammation. T follicular helper (Tfh) cells are relevant immunoregulators in cancer, and often correlate with better survival. How the Th2-skewed microenvironment in PDAC modulates the differentiation of Tfh cells and their immunoregulatory function is unknown.

**Methods** We carried out high-dimensional flow cytometry and T-cell receptor- and RNA-sequencing, as well as bioinformatics, immunohistochemistry and in vitro mechanistic studies.

**Findings** We identified Tfh1-, Tfh2-, and Tfh17-like cell clusters in the blood, tumors and tumor-draining lymph-nodes (TDLNs) of chemo-naïve PDAC patients and showed that high percentages of Tfh2 cells within the tumor tissue and TDLNs correlated with reduced patient survival. Moreover, only Tfh2 cells were highly activated and were reduced in frequency in patients who responded to neoadjuvant chemotherapy. RNA-sequencing analysis of immunoglobulin expression showed that tumor and TDLN samples expressed all immunoglobulin (*IGH*) isotypes apart from *IGHE*. Consistent with these findings, Tfh2 cells differentiated in vitro by tumor microenvironment-conditioned dendritic cells promoted the production of anti-inflammatory IgG4 antibodies by co-cultured B cells, dependent on IL-13. Moreover, unexpectedly, Tfh2 cells inhibited the secretion of pro-inflammatory IgE, dependent on prostaglandin $E_2$.

**Interpretation** Our results indicate that in PDAC, highly activated pro-tumor Tfh2 favor anti-inflammatory IgG4 production, while inhibit pro-inflammatory IgE. Thus, targeting the circuits that drive Tfh2 cells, in combination with chemotherapy, may re-establish beneficial anti-tumor Tfh–B cell interactions and facilitate more effective treatment.

**Funding** Research grants from the Italian Association for Cancer Research (AIRC) IG-19119 to MPP and the AIRC Special Program in Metastatic disease: the key unmet need in oncology, 5 per Mille no. 22737 to CB, MF, CD, MR and MPP; the ERA-NET EuroNanoMed III (a collaborative european grant financed by the Italian Ministry of Health, Italy) project PANIPAC (JTC2018/041) to MPP; the Fondazione Valsecchi to SC.



**Keywords:** Pancreatic cancer; Th2 inflammation; Tfh2; IgG4; IgE; $PGE_2$

*Corresponding author. Tumor Immunology Unit, Division of Immunology, Transplantation and Infectious Diseases, San Raffaele Scientific Institute, Via Olgettina 58, Milan 20132, Italy.
*E-mail address:* protti.mariapia@hsr.it (M.P. Protti).
[j]These authors contributed equally to this work.

## Research in context

### Evidence before this study

Pancreatic cancer is a very aggressive form of cancer that is characterized by predominant protumor Th2/M2-type inflammation. T follicular helper cells (Tfh) are required for antitumor B cell responses, and often their frequencies correlate with better survival in solid tumors. The presence of tertiary lymphoid structure–containing Tfh cells–and tumor-infiltrating B cells are reportedly associated with improved survival in neoplastic patients treated with immunotherapy. Nonetheless, pancreatic cancer responds poorly to immunotherapy. How the tumor microenvironment influences Tfh cell differentiation and functional activity in pancreatic cancer is unknown.

### Added value of this study

We found that in pancreatic cancer, at difference with other solid tumors and in the context of Th2/M2-type inflammation, the tumor microenvironment favors the priming of highly activated Tfh2 cells. The frequency of Tfh2 cells correlated with worse prognosis in chemo-naïve patients and was reduced in patients who responded to neoadjuvant chemotherapy. Tfh2 cells helped the secretion of anti-inflammatory protumor IgG4 and suppressed the induction of pro-inflammatory IgE. These data highlight the presence of dysfunctional Tfh–B cell interactions in pancreatic cancer and suggest the relevance of its distinctive immune contexture to explain the lack of response to immunotherapy.

### Implications of all the available evidence

Our study has immediate clinical implication for the treatment of pancreatic cancer patients. Indeed, targeting the inflammatory circuits that drive Tfh2 cells, in combination with chemotherapy, may re-establish beneficial anti-tumor Tfh–B cell interactions and facilitate more effective treatment.

## Introduction

Pancreatic ductal adenocarcinoma (PDAC) is a very aggressive form of cancer with dismal prognosis.[1,2] The tumor microenvironment of this cancer, characterized by a strong fibrotic stroma, exerts immunosuppressive activities[3] that support tumor cell growth, invasion and metastases. These activities are sustained by complex cross-talk between tumor cells, cancer-associated fibroblasts (CAFs), and immune cells. We[4–9] and others[10–17] have reported predominant Th2/M2-type inflammation in PDAC that correlates significantly with reduced patient survival.[5,7,16,18]

Ectopic lymphoid aggregates known as tertiary lymphoid structures (TLS) are frequently found in solid tumors, including PDAC,[19–23] and are believed to be active sites for anti-tumor immune responses.[24] TLS presence and tumor-infiltrating B cells are reportedly associated with improved survival in patients treated with immunotherapy.[24] Nonetheless, the use of immune checkpoint inhibitors to treat PDAC showed only limited efficacy in clinical studies.[3] Lack of efficacy of immunotherapy in this context might be associated with the presence of dysfunctional TLS and B cell responses. In this respect, T follicular helper (Tfh) cells are a crucial component of TLS.[25,26] These $CD4^+$ T cells constitute a specialized immune cell subset that provides help to B cells in the germinal centers of secondary lymphoid organs. Tfh cells are characterized by the expression of CXCR5, BCL6, PD-1, and ICOS and secretion of IL-21 and CXCL13.[25,26] Their presence in various solid tumors of non-lymphocytic origin, principally in germinal centers within TLS, frequently coincides with better prognosis.[27]

$CD4^+$ T cells sharing the phenotypic and functional properties of secondary lymphoid organ-associated Tfh cells have been found within the circulating memory $CD4^+CXCR5^+$ T-cell population. Based on the expression of CXCR3 and CCR6, three subsets can be distinguished: Tfh1 ($CXCR3^+CCR6^-$), characterized by lower helper capacity, and Tfh2 ($CXCR3^-CCR6^-$) and Tfh17 ($CCR6^+CXCR3^-$) subsets, characterized by higher helper capacity.[28] It remains to be established whether the three Tfh cell subsets are present within tumors, to form part of the tumor infiltrating-lymphocytes (TILs) population, or tumor-draining lymph-nodes (TDLNs). Moreover, it is unknown whether the three Tfh cell subsets have different effect on the anti-tumor immune response, and whether and how Th2-type inflammation in PDAC modulates Tfh cell subset differentiation and their immunoregulatory functions.

Here, we aimed to deepen our understanding of the immune contexture in PDAC through the characterization of the Tfh cell subsets, and potentially identify more favorable therapeutic avenues.

Using high-dimensional flow cytometry, we identified three clusters of Tfh-like cells–corresponding to Tfh1, Tfh2 and Tfh17 subsets–that were present in the blood, tumors, and TDLNs of PDAC patients. We determined their clonal expansion and recirculation between anatomical sites by T cell receptor sequencing (TCR-seq) and evaluated their correlation with the prognosis. Moreover, we determined the response of these cells to chemotherapy and conducted transcriptomic analyses to examine immunoglobulin (Ig) isotype expression in tumor samples. Finally, we conducted mechanistic studies to examine the effects of the

tumor microenvironment on the priming of Tfh cells with respect to B cell help.

## Methods

### Patient population

This observational prospective study included a total of 145 PDAC patients who were either chemo-naïve or had been treated with neoadjuvant chemotherapy (i.e., FOLFIRINOX or gemcitabine plus nab-paclitaxel) (see Supplementary Tables S1–S5 for the clinical characteristics of the patients).

### Patient sample collection

Blood, tumor, and TDLN samples were obtained from the different cohorts of PDAC patients. Sample size calculation was made based on the incidence and clinical management of the disease at San Raffaele Hospital.

### Blood, tumor, and TDLN processing

Peripheral blood mononuclear cells (PBMCs) were obtained from the venous blood of healthy donors (HDs) and PDAC patients by Ficoll-Hypaque (17144003, Cytiva) gradient stratification and cryopreserved. Tumor fragments and TDLNs selected by the pathologist were partly processed and partly snap frozen for RNA sequencing (RNA-seq) analyses. Tumor fragments were cut into small pieces, and placed in culture in serum-free medium X-VIVO20 (04-448Q, Lonza); TILs in the supernatant were collected 24 h later. TDLNs were perfused with 1x Non-enzymatic Dissociation Solution (C5914, Sigma-Aldrich), and the cells collected, washed and cryopreserved.

### Flow cytometry

The list of antibodies (Abs) used for flow cytometry and sorting is available in Supplementary Table S6. All Abs were titrated, and the appropriate saturating concentrations were used. Thawed PBMCs, TILs and TDLNs were incubated with the Abs against chemokine receptors at 37 °C for 20 min, washed and then labeled with a panel of surface phenotype Abs at room temperature for 20 min. After surface staining, cells were washed and incubated for 15 min with LIVE/DEAD markers to exclude dead cells. The samples were then fixed and permeabilized using the FoxP3 staining kit (00-5523-00, eBioscience) and incubated with intracellular Abs for 30 min. Finally, the cells were washed and stored in HBSS−/− (10-547F, Lonza) containing 2% human serum (14-490E, Lonza) and acquired on BD Symphony A5 or LSRII Fortessa instruments, using the setting previously described by Perfetto et al.[29] Data were analyzed using FlowJo software v10.8.0 (TreeStar). FACS-sortings were performed on MoFlo Astrios FACS sorter (Beckman Coulter).

### Unsupervised high-dimensional flow cytometry bioinformatic analysis

Flow cytometry data were imported into FlowJo software to compensate fluorescence spreading, and dead cells and debris were excluded from the analysis. Random down-sampling to 1000 events was performed for $CD3^+$ T- and $CD19^+$ B-cell populations, and the data were exported as Flow cytometry standard (FCS) files for further analysis in R software (version 4.0.2). Sample batches were read using read.flowSet (2.6.0) from the R package flowCore. We applied the logicle transformation, which allows the use of multiple samples to estimate transformation parameters. To reduce batch effects due to technical rather than biological variation, we normalized the signal of each marker using the gaussNorm function of the flowStat package (4.6.0). After batch-specific pre-processing, samples were concatenated into a SingleCellExperiment object in R using the prepData function of the CATALYST R package.[30,31] Dimensionality reduction by Uniform Manifold Approximation and Projection (UMAP) was subsequently applied to enable the visualization of the relative proximities of cells within reduced dimensions. We performed high-resolution, unsupervised clustering and meta-clustering using FlowSOM (2.2.0) and ConsensusClusterPlus (1.58.0) packages, following the workflow in Nowicka et al.[30] The T- and B-cell compartments were clustered based on the expression of 25 markers: CD3, CD4, CD8, CD45RO, CCR7, CCR6, CXCR3, CXCR5, PD-1, ICOS, BCL-6, CXCL13, CD57, TIM-3, GRANZYME-K, CD19, CD20, IgD, CD27, CD38, CD24, CD40, CD138, PDL-1 and HLA-DR.

### TCR-seq

Sequencing of the TCRβ chain was performed using chemo-naïve patient RNA (n = 4) obtained from Tfh cells FACS-sorted from different anatomical sites i.e., PBMCs, TDLNs and TILs (Supplementary Table S1). Tfh cells were identified as $CD4^+CD45RO^+CXCR5^+$ and sorted into Tfh1, Tfh2 and Tfh17 based on the expression of CXCR3 and CCR6 (Supplementary Figure S3a). Sequencing was performed using a modified RACE PCR protocol, independent of multiplex PCRs.[32,33] Samples were sequenced using the MiSeq platform (Illumina), and raw reads were sorted according to the individual barcode combinations used for each specimen. Analysis of the TCR clonotypes was carried out using MiXCR software[34] and VDJtool. Upon removal of the non-functional CDR3 amino acid sequences and frequency-based correction to eliminate erroneous clonotypes, only CDR3 clonotypes with sequence count >1 were further investigated. We analyzed the TCR repertoire clonality of overall Tfh cells isolated from the three anatomical sites and the CDR3 clonotypes (nucleotide sequences) identified at more than one anatomical site.

### RNA-seq of Tfh cells

Transcriptome analysis was performed on FACS-sorted Tfh cell subsets (as described above) from PBMCs obtained from HDs (n = 10), chemo-naive patients (n = 9), and patients treated with neoadjuvant chemotherapy (either FOLFIRINOX or gemcitabine plus nab-paclitaxel) (n = 10) from the Supplementary Table S1 cohort. RNA was extracted using the RNeasy Plus Mini or Micro kit (74134, Qiagen or 74034, Qiagen, respectively), based on cell number recovery. Before the preparation of RNA libraries for next-generation sequencing (NGS), total RNA quality was confirmed by running the samples on an RNA Pico Chip (Bioanalyzer 2100, Agilent). To generate the NGS libraries, we used the SMART-Seq v4 (TaKaRa) protocol, which allows mRNA library preparation starting from less than 2 ng of total RNA. Libraries of full-length double-stranded cDNA were fragmented and barcoded using Nextera XT (Illumina). Once the libraries were pooled, sequencing was run out using the Illumina NextSeq 500 sequencing system, generating ~20–30 M single-end reads, 75 nt long, for each sample.

### RNA-seq analyses of Tfh cells

RNA-seq analysis was performed as described previously,[35] with minor changes. Briefly, after quality filtering according to the Illumina pipeline, the 75-bp single-end reads were aligned to the reference human genome GRCh38 using STAR aligner (version 2.5.3a).[36] Only uniquely mapped reads were retained. At the gene level, expression counts were estimated using featureCounts (version1.6.3),[37] and annotated according to Gencode basic annotations (Gencode version 28). Both coding and noncoding genes were retained for downstream analyses. Prior to normalization using the DESeq2[38] "regularized log" transformation method (rlog), only genes with at least 1 count per million in at least 9 samples (the number in the smallest group) were retained. Analyses were performed separately for each Tfh subset and applied to the relevant dataset. rlog values were used as expression units, and less variable genes were filtered out, using the distribution of the median absolute deviation as a robust measure of variability.

### Co-expression network construction

The weighted gene co-expression gene analysis (WGCNA) R package was used to construct scale-free co-expression network for the retained genes.[39] A weighted adjacency matrix was built using a signed network and biweight midcorrelation to determine pairwise gene relationship. Then, using the power function β, a parameter to emphasize strong correlations and penalize weak correlations, the adjacency matrix was transformed into a topological overlap matrix (TOM), and the corresponding dissimilarity (1-TOM) was calculated. To cluster genes with similar expression profiles into gene modules, average linkage hierarchical clustering was performed on the dissimilarity matrix using the "cutreeDynamic" method with a minimum module size of 30 genes.

### Identification of phenotypically significant modules and their hub genes

To identify relevant modules, the Pearson correlations between module eigengenes (used as a measure of module expression in a given sample), and subject categories were calculated (after the creation of binary indicators for the categorical variables). To assess the significance, Student asymptotic p values for the given correlations were determined, choosing a cut-off of 0.05. Heatmaps representing the correlations between modules and subject categories were drawn using the ComplexHeatmap R package.[40] Hub genes were defined as those with the module membership >0.8.

### Pathway analysis

Ontology and pathway enrichment analysis were performed on the modules using the python package GSEApy, a python wrapper for Enrichr.[41] After the downloading of gmt files for the main databases and ontologies from the Enrichr website, highly specific or general terms (those with less than 5 or more than 500 genes) were filtered out, and the "enrichr" function applied by using the complete list of expressed genes as background set. A false discovery rate (Benjamini–Hochberg method) <0.05 was chosen as the cut-off criterion for multiple testing corrections, as the test was performed as many times as the number of gene sets in the selected public collections. Gene Ontology enrichment analysis on hub genes was performed using Gorilla.[42] REVIGO[43] was used to summarize Gene Ontology terms and reduce redundancy by selecting default parameters; the resulting list was set to "small size" for the brown hubs and "large size" for the magenta hubs.

### RNA-seq of whole tumor and TDLN tissues

Transcriptome analysis was performed on tumor samples from chemo-naïve patients (n = 21), FOLFIRINOX-treated patients (n = 19), gemcitabine + nab-paclitaxel-treated patients (n = 19), and TDLNs from chemo-naïve patients (n = 17) (Supplementary Table S7). RNA was extracted using the RNeasy Plus Mini kit (74134, Qiagen), and RNA samples were run on Tapestation 4100 (Agilent) to determine quality before library preparation for NGS. To generate the NGS libraries, we exploited the TruSeq Stranded mRNA (Illumina) protocol. This protocol allows unbiased 5'/3' library preparation starting from 100 ng of total RNA. Libraries were barcoded, pooled, and sequenced on an Illumina Nova-Seq 6000 sequencing system in the following mode: ~20–30 M single-end reads for each sample, 100 nt long. Demultiplexing and generation of fastq files were performed using bcl2fastq software (Illumina).

### RNA-seq analyses of whole tumor and TDLN tissue

RNA-seq analysis was performed as described previously,[35] with minor changes (see RNA-seq analyses of Tfh cells, above). Reads per kilobase of transcript per million reads mapped (RPKM) were computed for the expressed genes, and genes with at least 1 count per million in at least 19 samples (the number in the smallest group) were retained.

### B cell receptor (BCR) and somatic hypermutation (SHM) analyses

The BCR repertoire was reconstructed using TRUST4 algorithm,[44] starting with RNA-seq raw data (FASTQ) obtained for whole tumor and TDLN samples from chemo-naïve patients (Supplementary Table S7). Briefly, BCR sequences were determined by performing de novo assembly of V, J, and C genes, including the hypervariable CDR3, and reporting the consensus BCR sequences; contigs were then realigned to IMGT reference gene sequences. Repertoire diversity was assessed using the inverse Simpson's diversity index, according to the formula: $\frac{1}{\sum p_i^2}$, where $p_i$ is the proportional abundance of a clonotype. The index was computed at sample and isotype level by calculating the frequency of each clonotype after normalization of the transcript abundance, using the DESeq2 median of ratios method to account for sequencing depth and RNA composition. SHM rate was calculated by dividing the sum of mutational events for each clonotype at sample and isotype level by the number of clonotypes for that sample and isotype. The number of mutational events was obtained by comparing CDR3 nucleotide sequences pairwise and considering mutational events that differed by less than the number of nucleotides corresponding to 4% of the total length of the sequences. Wilcoxon signed-rank tests were performed to compare inverse Simpson values with a level of significance of 0.05.

### PDAC cell lines and CAF immortalization by huTERT transfection

Human PDAC cell lines BxPC-3, Capan-1, and A184 were obtained and cultured in IMDM (ECB2072L, Euroclone) with 10% FBS (FBS-11A, Capricorn Scientific), as described.[8] Primary CAFs, obtained from PDAC surgical samples as previously described,[5] were stably transfected to express the human telomerase reverse trancriptase gene (huTERT). Supernatant from the packaging Phoenix cell line transfected with pBabe-puro-hTERT (Plasmid #1771, Addgene) was used to infect CAFs at culture passage 3–4, and after 24 h puromycin (P8833, Sigma-Aldrich) selection was applied at 1.5 μg/ml (final concentration). Puromycin resistant colonies were checked for hTERT expression by Real Time-qPCR. PDAC and CAF cell lines were periodically tested for mycoplasma contamination using the MycoBlue Mycoplasma Detector kit (D101, Vazyme).

### Monocyte isolation

Monocytes were isolated from PBMCs in buffy coat samples from HDs by positive selection with CD14 MicroBeads (130-050-201, Miltenyi Biotec).

### Co-culture supernatants

Supernatants were obtained by co-culturing tumor cells with hTERT$^+$ CAFs and CD14$^+$ monocytes ($10^5$ cells/ml each, 1:1:1 ratio) in IMDM 10% FBS. After 48 h co-culture media were collected, centrifuged and filtered at 5 μm to obtain cell-free supernatants (Sup).

### Dendritic cell (DC) activation

PBMCs from HD buffy coats were enriched for myeloid DCs using the Pan-DC Enrichment Kit (130-100-777, Miltenyi Biotec) and purified by FACS-sorting, as described previously.[5,8] Then $5 \times 10^5$/ml DCs were cultured for 24 h in 96-well flat-bottom plates ±50 ng/ml Thymic Stromal Lymphopoietin (TSLP) (1398, R&D Systems), or Sup diluted 1:2 in X-VIVO 20 medium.

### DC:T cell co-culture

DC:T (1:5) co-cultures were set up, as described previously.[8] After 4–5 days of culture, cells were either collected for phenotypic FACS analysis, sorted for B cell help assays, or washed and seeded at $10^6$/ml 1:1 with anti-CD3/CD28-coated beads (130-091-441, Miltenyi Biotec) for 24 h restimulation. Supernatants were frozen before (for GM-CSF, IFN-γ, IL1-β, IL12p70, IL-13, IL-18, IL-2, IL-4, IL-5, IL-6 and TNF-α evaluation) and after (for IL-21 and prostaglandin $E_2$ ($PGE_2$) evaluation) restimulation for further analysis.

### T:B cell co-culture

After DC:T co-culture CD4$^+$ T cells were FACS-sorted into CD45RO$^+$ and CXCR5$^+$ or CXCR5$^-$ subpopulation, and autologous naïve B cells were isolated from PBMCs using the Naïve B cell Isolation kit II (130-094-131, Miltenyi Biotec). $5 \times 10^4$ B cells were added to sorted T cells in AIMV medium (0870112-DK, Gibco) with 1 μg/ml staphylococcal enterotoxin B (SEB) (S4481, Sigma-Aldrich). Naïve B cells treated with 0.5 μg/ml M-CD40L (ALX-522-110, Enzo Life Sciences) plus 2.5 μg/ml CpGB/ODN 2006 (tlr-2006-1, InvivoGen) or plus 50 ng/ml IL-13 (AF-200-13, Peprotech) and 20 ng/ml IL-21 (AF-200-21, Peprotech) were used as controls. At day 14, supernatants were collected and stored for Ig quantification. For IL13Rα2 functional blocking, 2.5 μg/ml of either goat IL13Rα2 (PA5-46976, Invitrogen) or isotype Goat Ig (AB-108-C, R&D Systems). Abs were added to the T:B co-culture on day 0. For $PGE_2$ functional assays, isolated B cells activated with M-CD40L, IL-13, and IL-21, as defined above, were treated ±1 μM $PGE_2$ (14010, Cayman Chemical), and ±1 μM $PGE_2$ receptor type 4 (EP4) antagonist (ONO-AE3-208, 3565, Tocris, Biotechne); culture supernatants were collected on day 10 for IgE and IgG4 quantification.

### Cytokine and Ig quantification

ELISAs were used for the quantification of TSLP (DY1398, R&D Systems), IL-1β, IL-13, IL-21 (3416-1H, 3471-1H, 3540-1H, Mabtech, respectively), $PGE_2$ (500141, Cayman Chemical), human IgE (ab195216, Abcam), and human IgG4 (88-50590, Invitrogen). ProcartaPlex human Th1/Th2 was used to detect GM-CSF, IFN-γ, IL1-β, IL12p70, IL-13, IL-18, IL-2, IL-4, IL-5, IL-6, and TNF-α (EPX110-10810-901, Thermofisher Scientific). The ProcartaPlex human isotyping assay (EPX070-10818-901, Thermofisher Scientific) was used for human Igs, and data were acquired and analyzed on the Luminex MAGPIX system (Luminex). Analytes below range concentration were not shown.

### Immunohistochemistry

Immunohistochemistry was performed on 5 µm serial sections of FFPE surgical specimens. Sections were immunostained using an automated immunostainer (BenchMark ULTRA; Ventana Medical Systems). Heat-induced antigen retrieval using cell conditioning solution CC1 (05279801001, Ventana Roche) was carried out before IgG4, CXCR5, GATA-3 and CD20 immunostaining, and protease 1 (05266688001, Ventana Roche) treatment was performed before IgG1 immunostaining. The primary Abs were anti-human IgG1 (19388, clone HP-6001, Sigma), anti-human IgG4 (760-4614, clone MRQ44, Roche-Ventana) mouse monoclonal Abs, CXCR5 (72172, clone D6L3C, Cellsignal), GATA-3 (PM405AA, clone L50-823 BioCare), and CD20 (05267099001, clone L26, Ventana-Roche). Ultraview Universal Dab detection Kit with diaminobenzidine development (05269806001, Ventana Roche) was used for detection.

### Statistics

Differences between two or more groups were statistically determined using the two-tailed Student *t*-test, Mann–Whitney test, Wilcoxon matched-pairs signed rank test or one-way ANOVA followed by Tukey's or Newman–Keuls multiple comparison test, as specified in the figure legends. Correlation analyses were performed using the two-tailed Pearson's correlation coefficient test. For survival analyses patients' follow-up started at the day of surgery till death or the last visit with patient alive (censored). Database lock was fixed four years after the beginning of the recruitment. Survival curves were estimated according to the Kaplan–Meier method and compared using the log-rank test, using the survfit and ggsurvplot functions of the survival and survminer R packages, respectively. A multivariate Cox regression analysis was performed with analyse_multivariate function of the survivalAnalysis R package, specifying the model: Surv(OS, Status) ~ Tfh2LowHigh + Sex + Age + Stage + MarginR. All the other statistical analyses were performed using GraphPad Prism (Version 6.0 software) (GraphPadSoftware, San Diego, CA, USA). A p value <0.05 was considered to be significant.

### Ethics

The Institutional Ethics Committee (Comitato Etico Fondazione Centro San Raffaele, Istituto Scientifico Ospedale San Raffaele, Milan, Italy) approved the study protocol (PDACTREAT), and informed consent was obtained from the donors.

### Role of the funding source

The funding source had no role in the study design, data collection, data analysis, interpretation of data, writing of the paper, or in decision to submit the paper for publication.

## Results

### High-dimensional flow cytometry identifies clusters of Tfh1-, Tfh2-, and Tfh17-like cells in the blood, TILs and TDLNs of chemo-naïve PDAC patients

In this study, we wished to deepen our knowledge of the immune contexture in PDAC. For this purpose, we developed a 25-marker panel (Supplementary Table S6) to evaluate the distribution of T- and B-cell subsets in the blood, TILs and TDLNs of PDAC patients (chemo-naïve or following neoadjuvant chemotherapy) (Supplementary Table S1) by ex-vivo high-dimensional flow cytometry. PBMCs from HDs were also used as controls (PBMC HD). Unsupervised analysis, based on dimensionality reduction by UMAP and high-resolution clustering using FlowSOM, detected the following cells in 22 clusters: naïve, central memory, and effector memory $CD4^+$ T cells (Fig. 1a and b and Supplementary Figure S1); naïve, central memory, effector memory and terminally differentiated $CD8^+$ T cells (Fig. 1a and Supplementary Figure S2a and b); and naïve and memory B cells and plasma cells/plasmablasts (Fig. 1a–c and Supplementary Figure S1). Clusters 12, 13, and 11 expressed markers corresponding to Tfh1 ($CXCR5^+$, $CXCR3^+$), Tfh2 ($CXCR5^+CXCR3^-CCR6^-$), and Tfh17 ($CXCR5^+CCR6^+$) subsets, respectively (Fig. 1a and b and Supplementary Figure S1). We then focused the analysis on chemo-naïve patients and HDs. Clusters 11 (Tfh17) and 13 (Tfh2) were present in PBMCs from HDs and all sample types from chemo-naïve patients, whereas cluster 12 (Tfh1) was mostly present in PBMCs and TILs from patients (Fig. 1d and e). The proportion of cluster 13 (Tfh2) in patients was significantly higher in TILs or TDLNs than PBMCs (Fig. 1e). Interestingly, in TILs from chemo-naïve patients, the proportion of cluster 13 (Tfh2) cells correlated significantly with that of cluster 3 cells, which expressed markers corresponding to plasma cells/plasmablasts (i.e., $CD3^-CD19^{+/-}CD20^-CD38^+CD138^+HLA\text{-}DR^{+/-}$) (Fig. 1a and c–f and Supplementary Figure S1). This finding suggested that these cells may mediate B cell help. By contrast, there was no correlation between the

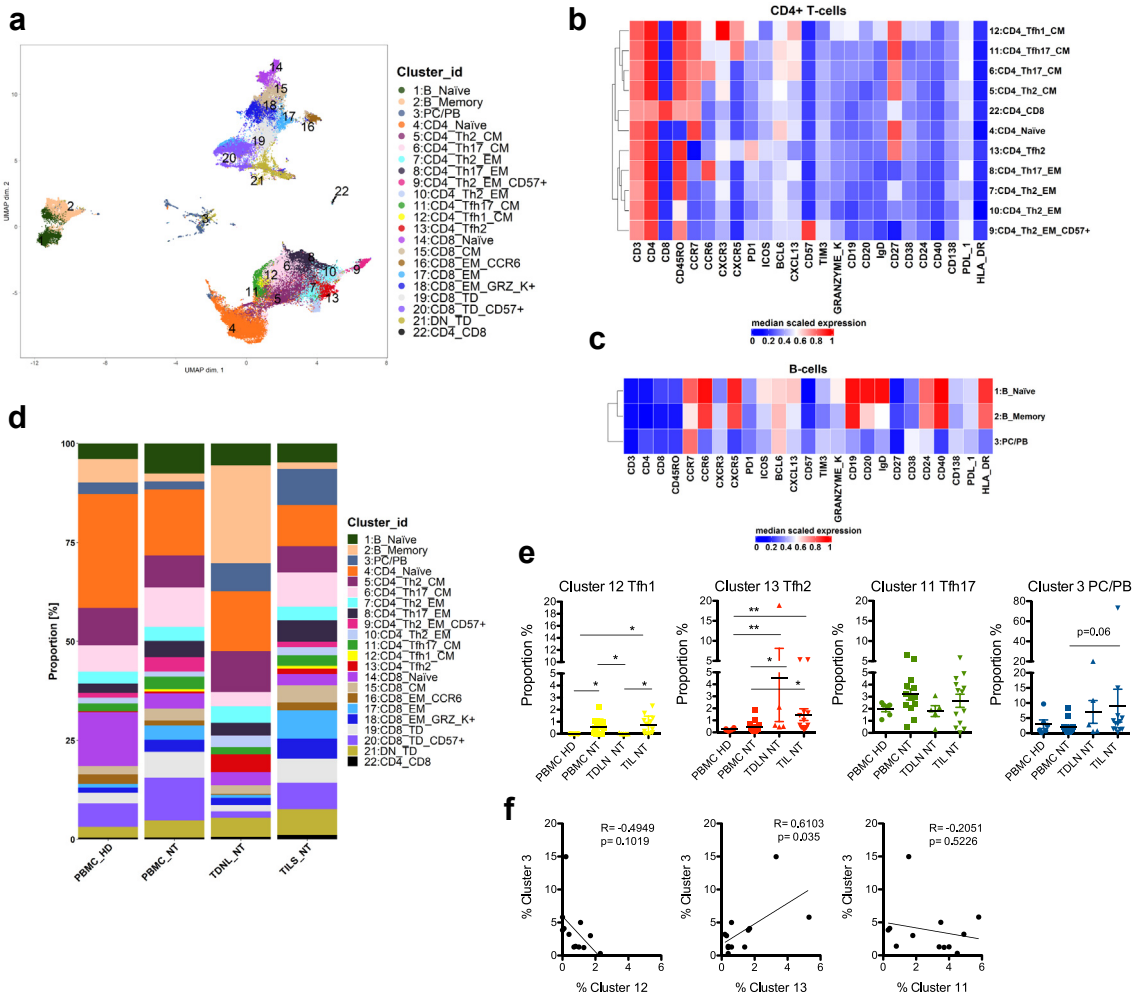


***Fig. 1:*** Unsupervised ex-vivo flow cytometry analysis of T- and B-cells in the blood, tumors and TDLNs of PDAC patients reveals clusters of Tfh1-, Tfh2-, and Tfh17-like cells. (a) Flow cytometry analyses were performed on PBMCs from HDs (n = 6) and the following matched samples: *i*) PBMCs (n = 13), TDLNs (n = 5) and TILs (n = 13) from chemo-naïve (NT = not treated) patients; *ii*) PBMCs (n = 11), TDLNs (n = 5), and TILs (n = 8) from patients treated with FOLFIRINOX; and *iii*) PBMCs (n = 14), TDLNs (n = 4), and TILs (n = 13) from patients treated with gemcitabine + nab-paclitaxel. The UMAP plot shows the T- and B-cell clusters of the merged samples; cell types are colored according to the 22 identified clusters. PC/PB = plasma cells/plasmablasts; CM = central memory; EM = effector memory; TD = terminally differentiated. (b and c) Heatmaps of median normalized expression of the markers used to annotate CD4 T-cell (b) and B-cell (c) clusters; heatmap color represents median marker expression (0–1), determined by logicle transformation. (d) Bar plots showing the percentages of individual clusters in the indicated NT specimen categories. (e) Percentages of cluster 12 (Tfh1), cluster 13 (Tfh2), cluster 11 (Tfh17), and cluster 3 (PC/PB) cells in the indicated NT specimens categories. Significance was calculated using the two-tailed Mann–Whitney test; *p < 0.05 and **p < 0.01. (f) Pearson correlation plots showing the relationship between cluster 3 (PC/PB) percentage and the percentage of cluster 12 (Tfh1), cluster 13 (Tfh2), or cluster 11 (Tfh17) within the TIL population of chemo-naïve patients.

proportions of clusters 11 and 12 (corresponding to the other Tfh cell subsets) and cluster 3.

### Tfh cells recirculate from tumors and/or TDLNs to blood, and high levels of Tfh2 cells correlate with reduced survival in chemo-naïve patients

To better characterize the identified Tfh cells, we used a gating strategy to identify the Tfh population and subsets (Supplementary Figure S3a) in a larger cohort of chemo-naïve patients (Supplementary Table S1). This analysis showed that Tfh cells, defined as $CD3^+CD4^+CD45RO^+CXCR5^+$, exhibited decreased frequency in patient blood compared to HD blood, instead accumulating in TILs and TDLNs (Supplementary Figure S3b). Evaluation of Tfh-related markers within the $CXCR5^+$-gated population showed that BCL6 levels were higher in patients than in HDs (Supplementary Figure S3c), whereas CXCL13 and IL-21 levels were

not significantly different (Supplementary Figure S3d and e). Tfh subsets were then identified based on the expression of CXCR3 and CCR6 or the co-expression of CD25 and FoxP3 (i.e., Tfh and regulatory [Tfr] subsets, respectively) (Supplementary Figure S3a). In PBMCs from HDs and patients, the proportions of Tfh2 and Tfh17 cells within the CXCR5$^+$ population were increased relative to the proportion of Tfh1, whereas similar proportions of these subtypes were observed in TILs and TDLNs. Tfr frequency was almost negligible in all categories (Fig. 2a).

As TLS, where Tfh cells are mainly located, are important sites for the initiation and/or maintenance of local and systemic anti-tumor T- and B-cell responses,[45] we wanted to evaluate the extent of recirculation of Tfh cells from tumor tissue and/or TDLNs (both potentially sites of antitumor response induction) to blood. Therefore, we FACS-sorted Tfh cells from four matched sets of chemo-naïve patient blood, TIL, and TDLN samples (Supplementary Table S1) and performed high-throughput TCR-seq on the isolated RNA. We found the highest percentages of expanded clonotypes among TILs, followed by PBMCs and TDLNs (Fig. 2b). Importantly, we identified Tfh cells with identical TCR beta chains that were shared between blood and TDLNs, blood and TILs, TILs and TDLNs, as well as between all three sites (Fig. 2c and Supplementary Figure S4), suggesting their recirculation between the three anatomical sites.

We then evaluated the clinical relevance of the occurrence of Tfh cells in the blood, tumors and TDLNs of chemo-naive patients (Supplementary Tables S2 and S3). Patients were grouped according to the median percentages of CXCR5$^+$ cells, or Tfh1/Tfh2/Tfh17 cell subsets in the three anatomical sites. We found that patients with Tfh2 cell percentages below median values in tumors or TDLNs survived significantly longer than patients with Tfh2 cell percentages above median values (Fig. 2d, middle and right). The same trend was observed for Tfh2 cells in the blood (Fig. 2d, left). By contrast, percentages of CXCR5$^+$ cells or Tfh1/Tfh17 cells did not significantly impact patient survival (Supplementary Figure S5). Multivariate analyses stratification for sex, age, tumor stage, and surgical margins confirmed that the percentage of Tfh2 cells (low/high categorical covariate) in tumors and TDLNs was independently predictive of overall survival (Supplementary Tables S4 and S5).

### Tfh2 cells are highly activated and their frequency is reduced after neoadjuvant chemotherapy

Having shown that out of the three Tfh subsets, only Tfh2 showed clinical relevance, we wanted to investigate the activation status of the three Tfh subsets in chemo-naïve patients. Indeed, unsupervised analyses had already shown that cluster 12 (Tfh1) and cluster 11 (Tfh17) presented central memory phenotypes, whereas cluster 13 (Tfh2) presented an effector memory phenotype (Fig. 1b, and Supplementary Figure S1). We went on to evaluate the distribution of Tfh subsets expressing different levels of PD-1 (Supplementary Figure S6a). Notably, the frequency of Tfh2 cells expressing high levels of PD-1 was significantly higher in patients (all sample types) than in HDs (blood) (Supplementary Figure S6b), whereas the distribution of Tfh1 and Tfh17 subsets was similar in all samples. Moreover, cells expressing low PD-1 levels did not show any differences in Tfh subset distribution (Supplementary Figure S6c). We then compared the proportions of highly activated Tfh cells co-expressing high levels of PD-1 and ICOS (i.e., PD-1$^{++}$/ICOS$^+$, Fig. 3a) in blood from HDs and blood, TILs and TDLNs from PDAC patients. Similar to the results above, only Tfh2 subset exhibited significantly increased frequency in patient samples (Fig. 3b, middle). Importantly, highly activated Tfh2 cells from patients were increased at all anatomical sites, while highly activated Tfh17 cells showed significantly decreased frequency, compared with both Tfh1 and Tfh2 subsets (Fig. 3c).

Next, we considered the distribution of highly activated Tfh subsets in patients with borderline resectable or locally advanced cancer who met the criteria for surgery after neoadjuvant chemotherapy (Supplementary Table S1). We found that highly activated Tfh2 cells were decreased in frequency at all anatomical sites in chemotherapy-treated patients compared with chemo-naïve patients (Fig. 4a–c, middle panels). Moreover, this effect was more evident after treatment with gemcitabine plus nab-paclitaxel than after FOLFIRINOX. Overall, chemotherapy did not substantially change Tfh1 and Tfh17 subset distribution, although, increased frequency of Tfh17 cells was observed in the TDLNs of patients treated with gemcitabine plus nab-paclitaxel (Fig. 4a–c, left and right panels). Notably, when patients were grouped as responders (score 1) and non-responders (score 0) to chemotherapy, based on criteria defined previously,[46] we observed reduced percentages of Tfh2 cells in the tumors of responders (Fig. 4d). In support of the higher modulatory effect of gemcitabine plus nab-paclitaxel, the correlation between Tfh2 cells (cluster 13) and plasma cells/plasmablasts (cluster 3) in the tumors, observed in chemo-naïve patients (Fig. 1f), was lost in patients treated with gemcitabine plus nab-paclitaxel but not with FOLFIRINOX (Fig. 4e).

To further characterize potential differences within the Tfh subsets, we performed transcriptomic analyses on FACS-sorted Tfh1, Tfh2, and Tfh17 subsets isolated from the blood of HDs and chemo-naïve or chemotherapy-treated patients (Supplementary Table S1). We decided to perform these analyses on Tfh cell isolated from PBMCs and not from the tumor because i) the yield of cells obtained from chemotherapy-treated tissue samples was too low for

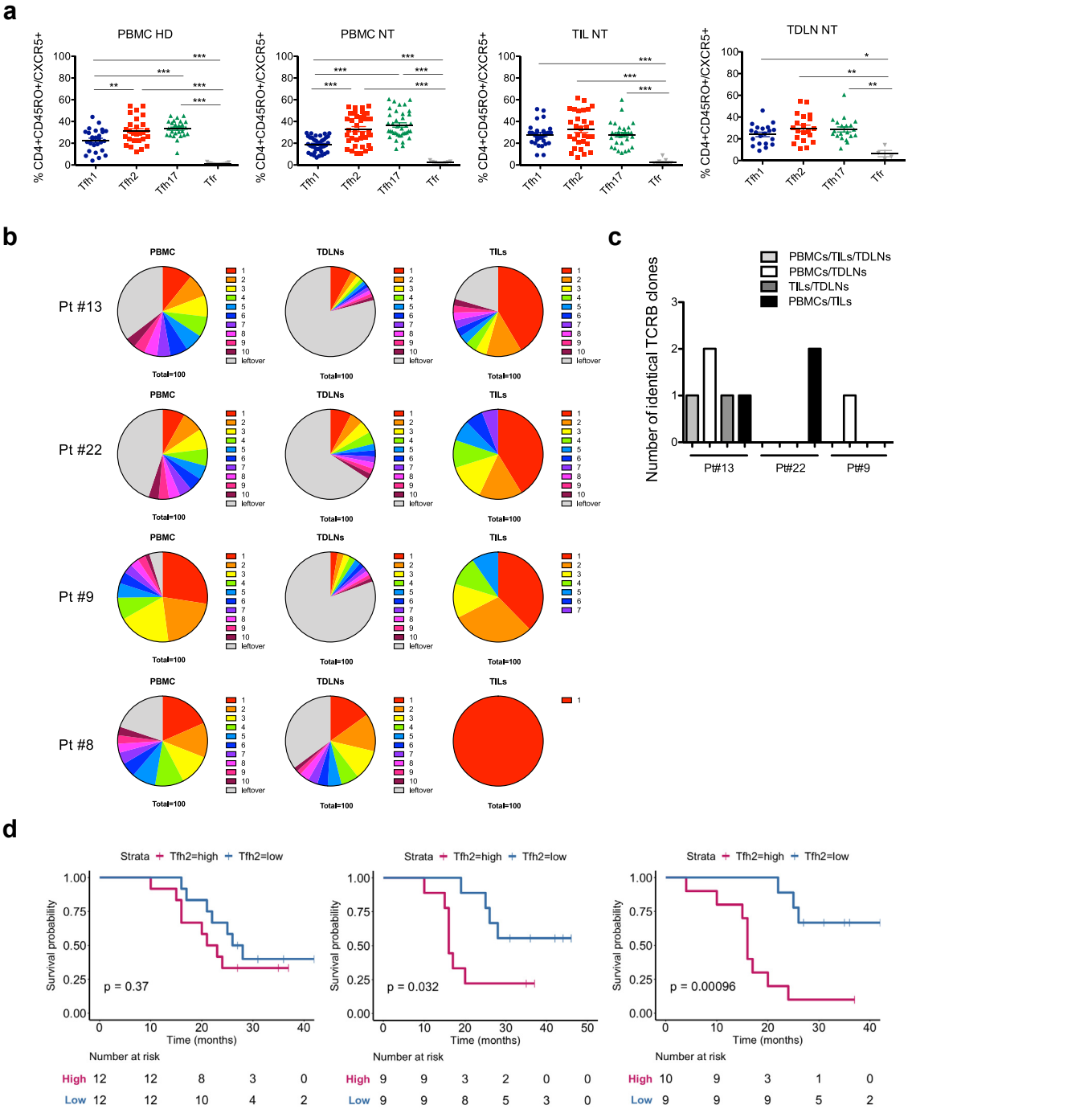


***Fig. 2:*** Tfh1, Tfh2 and Tfh17 cells recirculate between blood, tumor, and TDLNs in chemo-naïve patients, and Tfh2 cells negatively correlate with patient survival. (a) Tfh subset distribution within PBMCs from HDs (n = 27; for Tfr, n = 13), and PBMCs (n = 38; for Tfr, n = 9); TILs (n = 30; for Tfr, n = 9), and TDLNs (n = 20; for Tfr, n = 4) from chemo-naïve patients (NT). Significance was calculated using one-way ANOVA followed by Tukey's multiple comparison test; *p < 0.05, **p < 0.01, ***p < 0.001. (b) Pie charts represent the distribution of the 10 most predominant clonotypes in the TCR beta chain repertoire of Tfh cells retrieved from the three anatomical sites. Color coding indicates the relative contribution of each CDR3 nucleotide sequence to the total TCR repertoire; the larger the grey slice, the more polyclonal the TCR repertoire. (c) Numbers of clones with identical CDR3 amino-acid sequences shared between the three anatomical sites. (d) Kaplan–Meier curves for the overall survival of chemo-naïve patients according to the median percentage of Tfh2 cells in PBMCs (n = 24) (left), TILs (n = 18) (middle), and TDLNs (n = 19) (right). Significance was evaluated using the log-rank (Mantel–Cox) test.

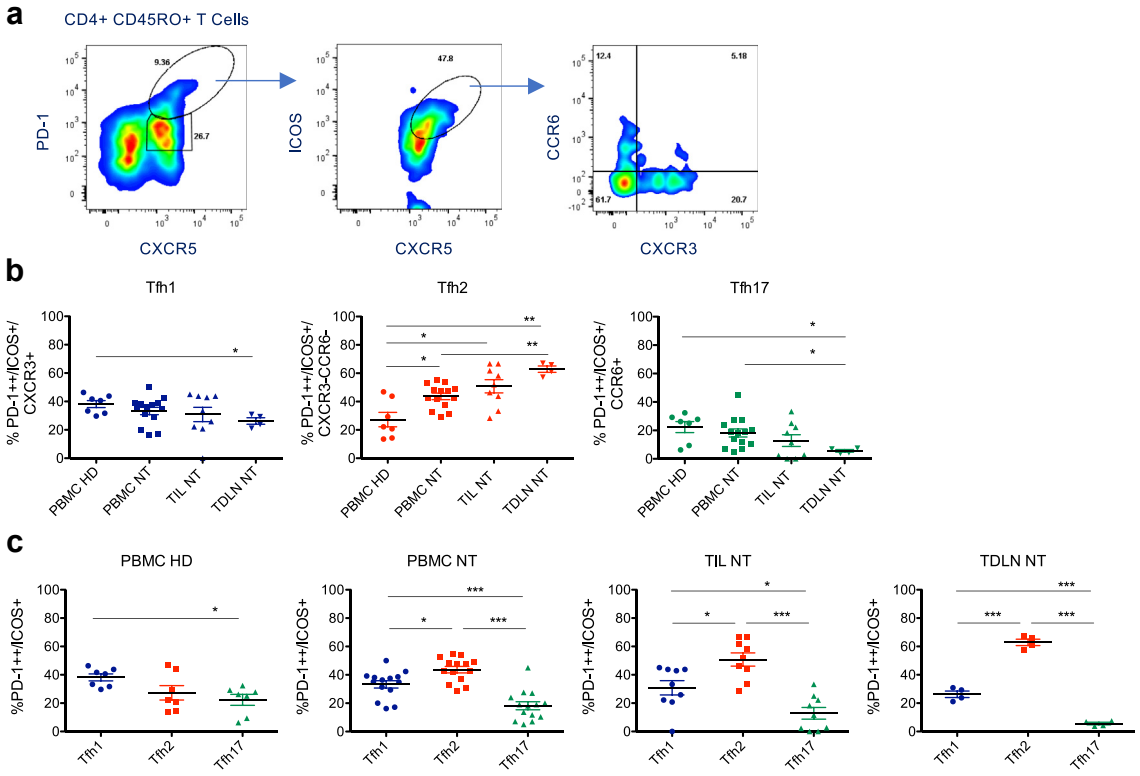


*Fig. 3:* Tfh2 cells are highly activated in chemo-naïve PDAC patients. (a) Gating strategies to identify activated Tfh cells within the $CD4^+$/$CD45RO^+$ population based on $CXCR5^+$, PD-1 ($PD\text{-}1^{++}$ and $PD\text{-}1^+$), and $ICOS^+$ expression. Highly activated Tfh cells were identified as $PD\text{-}1^{++}$/$ICOS^+$ cells, and Tfh1, Tfh2, and Tfh17 subsets were further identified based on CCR6 and CXCR3 expression. (b) Frequency of highly activated Tfh subsets in PBMCs from HDs (n = 7), and PBMCs (n = 14), TILs (n = 9) and TDLNs (n = 4) from chemo-naïve (NT) patients. Significance was calculated using the two-tailed Mann–Whitney test; *p < 0.05 and **p < 0.01. (c) Distribution of highly activated Tfh subsets in PBMCs from HDs (n = 7), and PBMCs (n = 15), TILs (n = 9) and TDLNs (n = 4) from chemo-naïve (NT) patients. Significance was calculated by one-way ANOVA followed by Tukey's multiple comparison test; *p < 0.05, **p < 0.01, ***p < 0.001.

reliable testing, ii) the distribution of highly activated Tfh2 cells was similar in patient PBMCs, TILs and TDLNs, iii) Tfh cells sharing the same TCR recirculated from tumor and TDLNs and blood were identified, and iv) the possible comparison also with Tfh cells isolated from HDs. We conducted WGCNA, building distinct co-expression networks for each Tfh subset, to enable the investigation of specific programs associated with Tfh cell activation. Having obtained several modules of co-expressed genes for each Tfh subset, we correlated modules with the categories using the WGCNA module eigengene and determined pathway enrichment in each module (Supplementary Tables S8–S10). Notably, only the Tfh2 modules exhibited significant correlations with the chemo-naïve patient category (Fig. 5a). Moreover, pathway enrichment analysis indicated the upregulation of genes related to T cell activation and inflammatory responses in Tfh2 cells (Fig. 5a, annotated on the right). We then identified the hub genes for the Tfh2 subset and performed gene ontology analyses that, in the brown and magenta modules (Supplementary Table S11), resulted in the identification of biological processes that included regulation of gene expression, immune effector processes, T cell differentiation, cytokine secretion (Fig. 5b, left), and metabolic processes (Fig. 5b, right). Collectively, transcriptomic analyses strongly supported the higher activation status, including proliferative, metabolic and effector functions, of Tfh2 cells in comparison with the Tfh1/Tfh17 subsets.

### IgA and all IgG isotypes, but not IgE, are expressed in tumor and TDLN tissues, and IgG1 and IgG4 colocalize within tumor cell nests

To gain insights on the Tfh cell functional activity, we wanted to evaluate the presence and distribution of different Ig isotypes in PDAC. We conducted RNA-seq on surgical specimens from either chemo-naïve PDAC patients (tumor and TDLN samples) or chemotherapy-treated patients (tumor samples only); the latter received FOLFIRINOX or gemcitabine plus nab-paclitaxel (Supplementary Table S7). Analysis of *IGH*

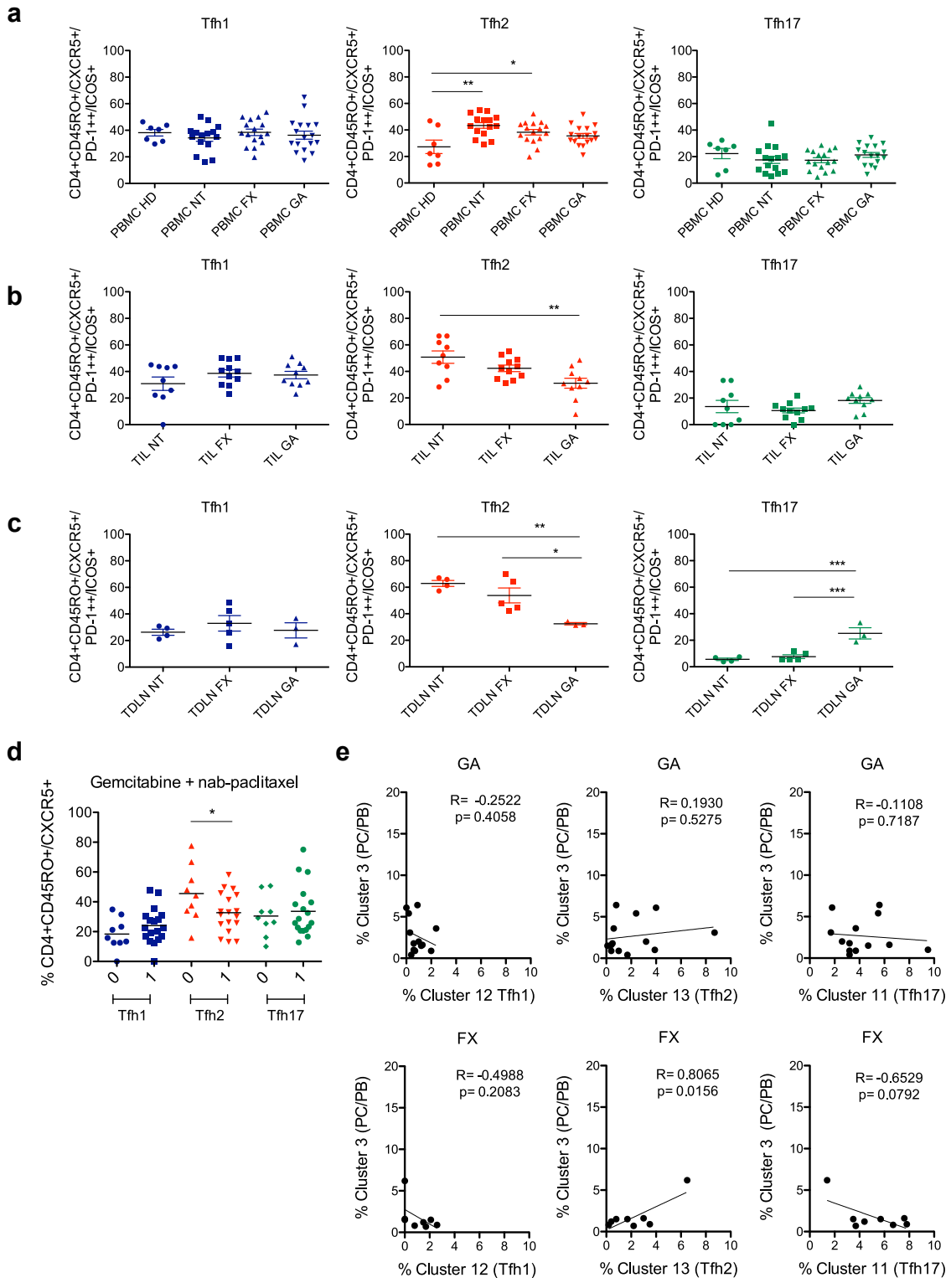


*Fig. 4:* Tfh subset distribution in PBMCs, TILs and TDLNs from chemo-naïve vs chemotherapy-treated PDAC patients. (a–c) Percentages of highly activated Tfh1, Tfh2 and Tfh17 cells in (a), PBMCs from HDs (n = 7), chemo-naïve (NT) patients (n = 15) and patients treated with FOLFIRINOX (FX, n = 16); or gemcitabine plus Abraxane (nab-paclitaxel) (GA, n = 17)) patients; (b) TILs from chemo-naïve (NT, n = 9) vs chemotherapy-treated patients (FX, n = 11; GA n = 10); and (c) TDLNs of chemo-naïve (NT, n = 4) vs chemotherapy-treated (FX, n = 5; GA, n = 3) patients.

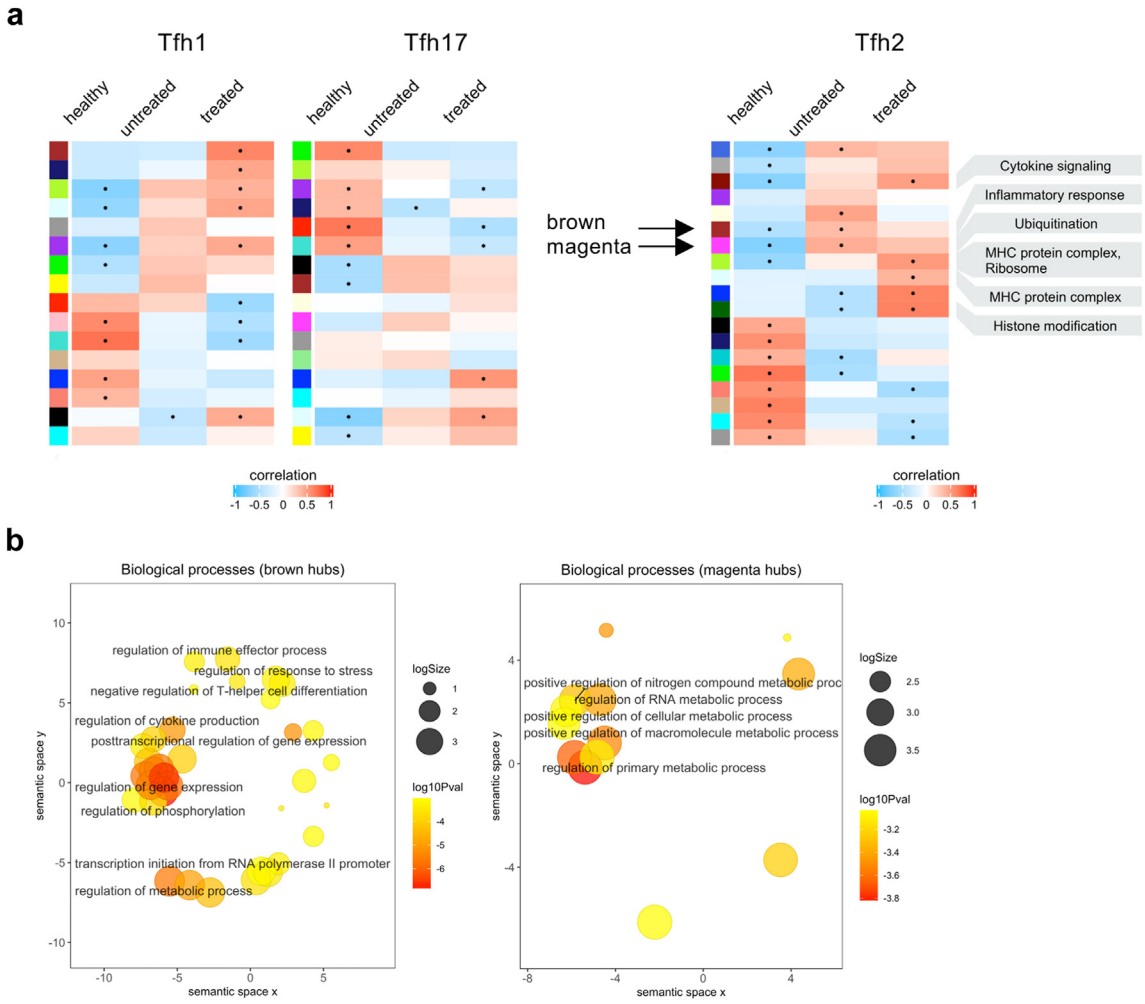


***Fig. 5:*** Co-expression networks of circulating Tfh1, Tfh2 and Tfh17 subsets. (a) Tfh1, Tfh2, and Tfh17 subsets FACS-sorted from the blood of HDs (n = 10), chemo-naïve (n = 9), and chemotherapy-treated (n = 10) PDAC patients were subject to RNA-seq analyses. The heat map shows the WGCNA modules for Tfh1 and Tfh17 (left) and Tfh2 (with annotated enrichment analyses, right). Black stars represent transcriptional networks showing significant correlation with the indicated category (healthy, untreated, treated), calculated using the Student asymptotic p-value for the given correlation (cut-off of 0.05). (b) Gene ontology categories associated with hub genes in the relevant modules. Left panel = brown module; right panel = magenta module.

isotype distribution in chemo-naïve patient tumor (Fig. 6a, upper panel) and TDLN (Fig. 6a, lower panel) samples revealed high levels of expression of all the immunoglobulin *(IGH)A* and *IGHG* isotypes, contrasting with remarkably lower/absent expression of *IGHE*.

To further characterize the features of the Ig isotypes detected in tumor and TDLN tissues, we went on to analyze the BCR sequences using the TRUST algorithm.[44] This analysis revealed a higher diversity index for *IGHG1*, compared with all other *IGHG* isotypes, both in tumors and in paired TDLNs (Fig. 6b). SHM and affinity maturation by BCR mutagenesis in the germinal centers generate B cell clones with high affinity. Evaluation of SHM in different *IGHG* isotypes showed that

Significance was calculated using one-way ANOVA followed by the Tukey's multiple comparison test; *p < 0.05 and **p < 0.01. (d) Tfh subset distribution in the TILs of GA-treated patients (n = 27) based on pathological response to chemotherapy. 0 = no or minimal response (n = 9), 1 = minimal to marked response (n = 18). Significance was calculated using the two-tailed unpaired Student's t-test; *p < 0.05. (e) Pearson correlation plots showing the relationship between cluster 3 (PC/PB) percentage and the percentage of cluster 12 (Tfh1), cluster 13 (Tfh2), or cluster 11 (Tfh17) cells in patients treated with GA (upper panels) or FX (lower panels).

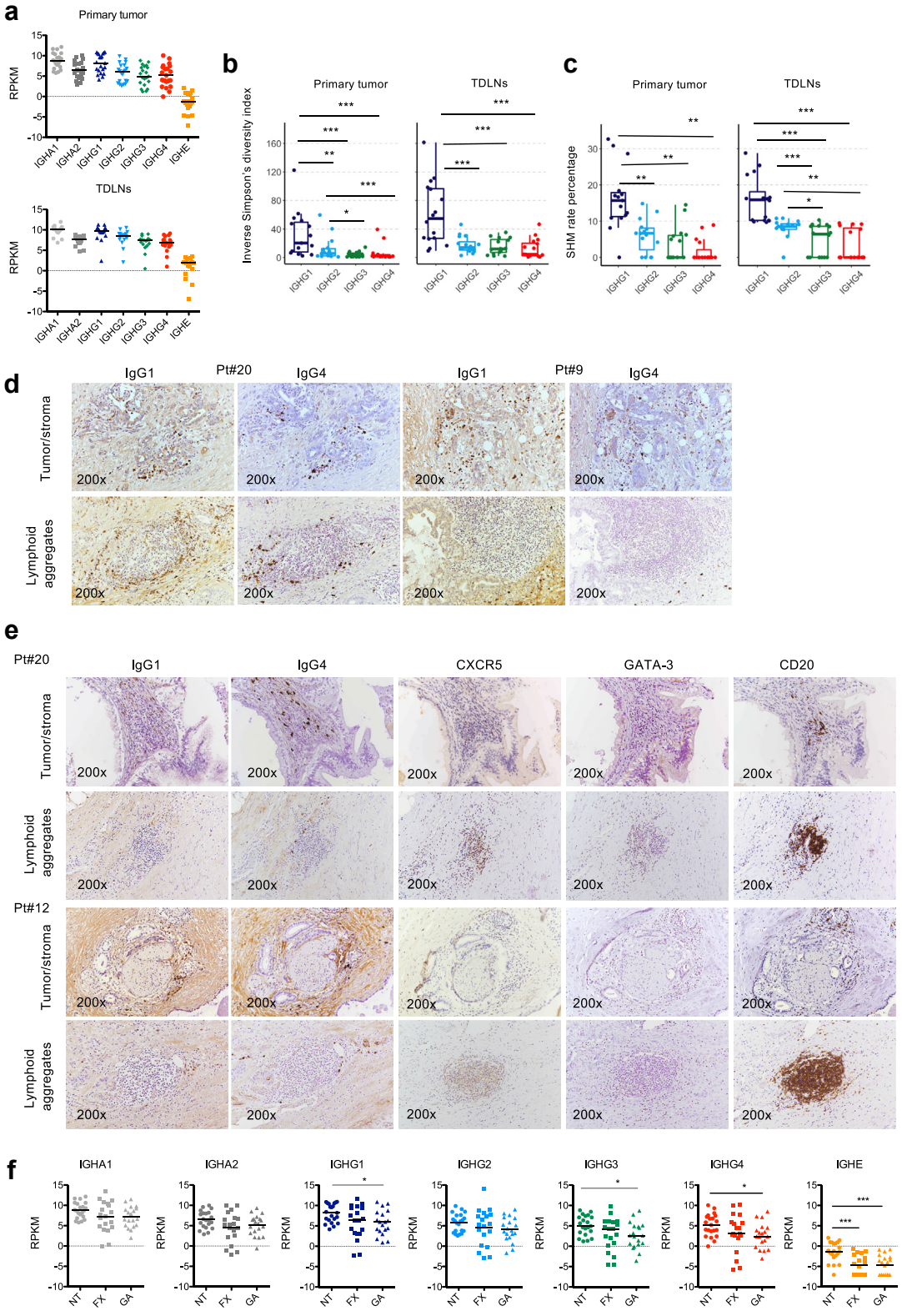


*Fig. 6:* Ig features in chemo-naïve and chemotherapy-treated surgical samples. (a) RNA-seq data were obtained from surgical specimens. Plots indicate the expression of *IGH* isotypes in tumor (n = 21) and TDLN (n = 17) samples from the chemo-naïve patient cohort (Supplementary

*IGHG1* exhibited the highest maturation rate in both tumors and TDLNs (Fig. 6c).

We then performed immunohistochemistry to determine the spatial distribution of IgG1 and IgG4 in tumors from chemo-naïve cohort patients (Supplementary Table S1). Detection of the two IgG isotypes in serial sections confirmed the transcriptomic data, with distribution in both lymphoid aggregates (particularly around the edges) and tumor/stroma. Moreover, in several areas IgG1 and IgG4 appeared to co-localize within tumor cell nests (Fig. 6d and e). The presence of bona fide Tfh2 cells (i.e., $CXCR5^+GATA\text{-}3^+$) and B cells (i.e., $CD20^+$) was also evaluated. In lymphoid aggregates $CD20^+$ cells were highly represented, $CXCR5^+GATA\text{-}3^+$ cells were also present and localized close to the IgGs. In the tumor/stroma $CD20^+$, $CXCR5^+$ and $GATA3^+$ cells were more rare and scattered, and were localized in the same areas of IgGs (Fig. 6e). Collectively, these data suggest that interactions between Tfh and B cells with production of Ig develops mainly in lymphoid aggregates, and IgG1 and IgG4 positive plasma cells migrate from the lymphoid aggregates to the tumor/stroma where they co-localize in several areas within tumor cell nests.

Finally, to evaluate the effects of neoadjuvant chemotherapy on Ig isotype distribution we compared *IGH* expression in samples from chemo-naïve and chemotherapy-treated patients. For all *IGHG* isotypes, we identified a trend of reduced expression in chemotherapy-treated patients, which reached significance for *IGHG1*, *IGHG3*, and *IGHG4* in samples from patients treated with gemcitabine plus nab-paclitaxel (Fig. 6e). The already almost negligible expression values of *IGHE* were further reduced in samples from patients treated with both chemotherapeutic regimens.

### Tumor microenvironment-mediated priming of Tfh2 cells in vitro induces isotype switching to IgG4 and $PGE_2$-dependent inhibition of IgE secretion in co-cultured B cells

TSLP has been reported to promote Tfh2 cell differentiation in Th2-skewed environments.[47] We previously reported that the predominance of Th2-type inflammation in PDAC depended on complex crosstalk within the tumor microenvironment involving TSLP secretion by CAFs,[5,6] in response to IL-1 released by tumor cells and tumor-associated macrophages.[8] To evaluate the involvement of the tumor microenvironment in Tfh cell priming and Tfh2 differentiation, we developed an in vitro assay that mimicked its effects through the co-culturing of tumor cells, CAFs and monocytes; the resulting culture supernatant was then used to condition myeloid DCs (Sup-DCs) (Fig. 7a). As suggested by our previous studies,[5,8] the supernatant contained IL-1β and TSLP (Supplementary Figure S7). Subsequently, we co-cultured the Sup-DCs with naïve $CD4^+$ T cells, and tested the differentiation of $CXCR5^+$ T cells, as well as their phenotypic and functional properties. In line with the ex-vivo data, we observed memory $CD4^+CXCR5^+$ cells expressing differing levels of PD-1 ($high^{++}$, $low^+$), while Tfh2 cells predominated within the highly activated ($PD\text{-}1^{++}ICOS^+$) Tfh cells subpopulation (Fig. 7b). The percentage of $BCL6^+$ cells was also higher within this highly activated subpopulation, whereas $CXCL13^+$ cell percentages were comparable in the $PD\text{-}1^{++}ICOS^+$ and $PD\text{-}1^+ICOS^+$ subpopulations (Fig. 7b). Analysis of cytokine secretion showed that Tfh cells differentiated in vitro with Sup-DCs released more IL-21 than Tfh cells differentiated by co-culturing with TSLP-stimulated DCs (TSLP-DCs; Fig. 7c). In addition, Sup-DCs promoted the release of significantly higher levels of IL-13 than of IFN-γ, and of GM-CSF, IL-2, or TNF-α, and, unlike TSLP-DCs, of IL-6 (Fig. 7d).

Next, we co-cultured FACS-sorted Sup-DC-primed $CXCR5^+$ and $CXCR5^-$ cells with autologous naïve B cells to test their B cell help activity. $CXCR5^+$ T cells were much more effective than $CXCR5^-$ T cells in inducing secretion of IgG1, IgG2, IgG3, IgG4, and IgA by B cells, whereas IgE secretion was not induced (Fig. 7e and Supplementary Figure S8). Importantly, B cell help for IgG4, but not other isotypes, was inhibited in the presence of an anti-IL-13Rα2 Ab (Fig. 7e and Supplementary Figure S8). The lack of IgE secretion induced by in vitro differentiated predominantly Tfh2 cells agreed with the ex-vivo *IGHE* expression data (Fig. 6a), but contrasted with results obtained using Tfh2 cells differentiated in vitro with TSLP-DCs.[47] As IgE antibodies (Abs) have features of anti-tumor effectors,[48] we hypothesized that factor(s) released by Tfh2 cells could be actively involved in inhibiting IgE secretion, as a potential mechanism of immune evasion. For example, prostaglandins are critical lipid mediators

Table S7). (b and c) BCR analyses in paired tumor and TDLN samples from chemo-naïve patients (n = 17). Inverse Simpson's diversity index (b) and SHM rate (c) for each *IGHG* isotype. Significance was calculated using the Wilcoxon matched-pairs signed rank test; *p < 0.05, **p < 0.01, ***p < 0.001. (d) Immunohistochemical analysis of the spatial distribution of IgG1 and IgG4 in lymphoid aggregates and stroma in chemo-naïve surgical samples (serial sections); n = 5, two representative cases (Pt#20 and Pt#9) are shown. (f) Immunohistochemical analysis of the spatial distribution of IgG1 and IgG4, and $CXCR5^+$, $GATA\text{-}3^+$, and $CD20^+$ cells in lymphoid aggregates and stroma in chemo-naïve surgical samples (serial sections); n = 5, two representative cases (Pt#20 and Pt#12) are shown. (e) RNA expression of the indicated *IGH* isotypes (determined by RNA-seq) in tumor samples from chemotherapy-treated (FOLFIRINOX [FX], n = 19; Gemcitabine plus Abraxane [GA], n = 19) and chemo-naïve (n = 21) patient cohorts (Supplementary Table S7). Significance was calculated using the two-tailed Mann–Whitney test; *p < 0.05 and ***p < 0.001.

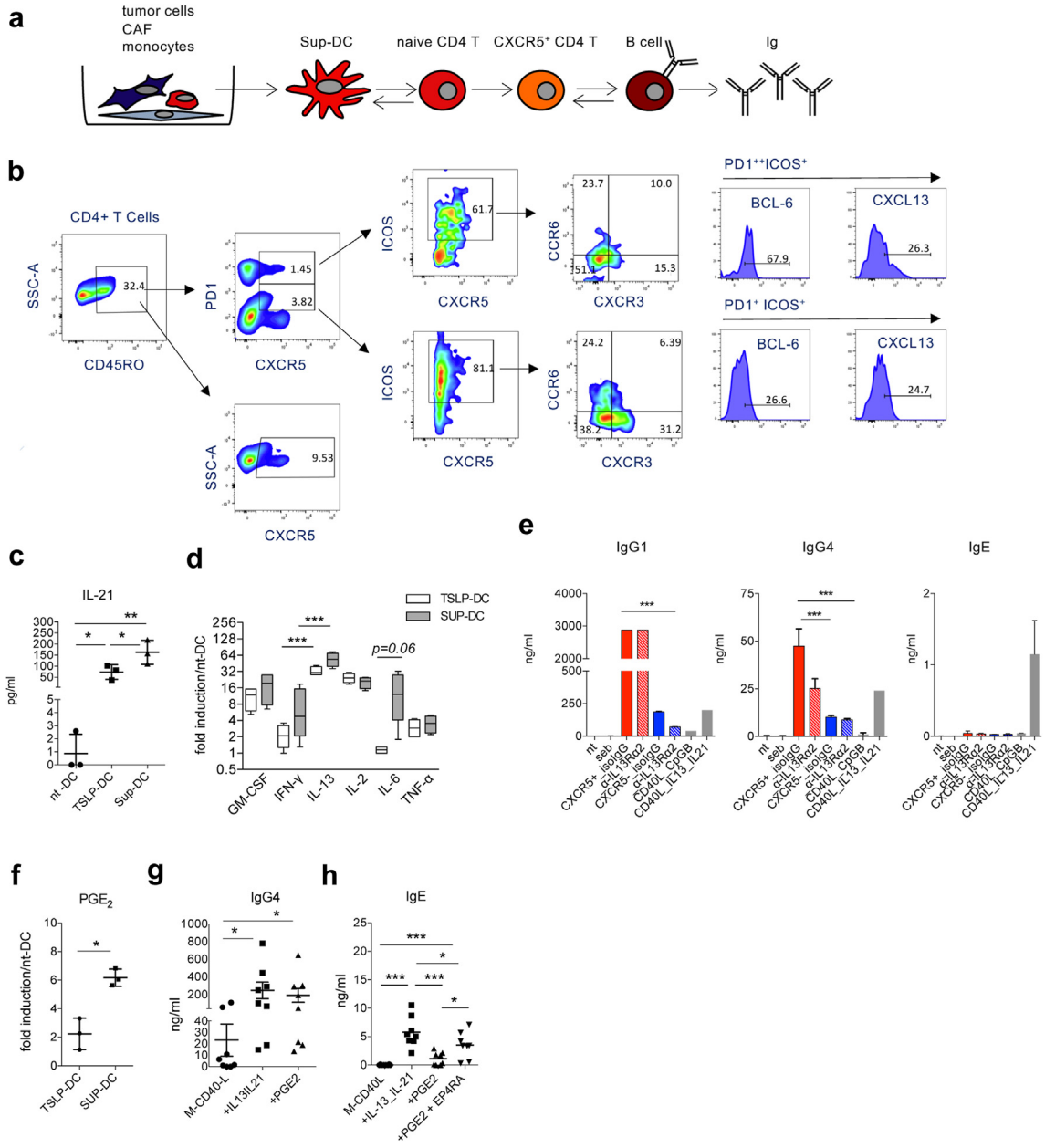


***Fig. 7:*** In vitro-differentiated Tfh2 cells promote IgG4 and inhibit IgE secretion by B cells. (a) Experimental scheme: conditioned medium from co-cultures of tumor cells (BxPC3), CAFs, and primary monocytes was used to condition myeloid DCs (Sup-DC), which, in turn, were used to prime naïve $CD4^+$ T cells. Untreated myeloid DCs (nt-DC) and TSLP-treated myeloid DCs (TSLP-DC) were used as controls. (b) Flow cytometry analysis of in vitro differentiated $CXCR5^+$ T cells; contour plots and histograms show expression of PD-1 (high and low), ICOS, BCL6, CXCL13, and differentiation into Tfh1, Tfh2 and Tfh17 cells, based on CCR6 and CXCR3 (representative of n = 3). (c and d), Secretion of IL-21 (n = 3) (c), and other cytokines (d) by in vitro primed $CD4^+$ T (predominantly Tfh2) cells activated as indicated. Results are expressed as fold increases in cytokine secretion relative to levels in nt-DC:T co-cultures (n = 4). (e) B cell help mediated by FACS-sorted $CXCR5^+$ (red) and $CXCR5^-$ (blue) T cells in the absence/presence of an anti-IL-13Ra2 Ab (dashed columns) or an isotype control Ab (filled columns); representative of n = 2. CD40L + CpGB and CD40L + IL-13 + IL-21 were used as positive controls. (f) $PGE_2$ secretion by in vitro-primed (TSLP-DC or Sup-DC) predominant Tfh2 cells, expressed as fold increases over $PGE_2$ levels produced by nt-DC:T co-cultures (n = 3). (g) IgG4 secreted by B cells cultured with CD40L alone or CD40L + IL-13 + IL-21 in the presence/absence of $PGE_2$ (n = 8). (h) IgE secreted by B cells cultured as in (g) without/with the EP4 receptor antagonist (EP4RA). Significance was calculated using the paired Student's *t*-test in (f) or one-way ANOVA followed by Newman–Keuls multiple comparison test in (c–e) and (g and h); *p < 0.05 and ***p < 0.001.

released during type-2 inflammation,[49] and a role for $PGE_2$ in inhibiting IgE secretion by human activated B cells has been reported.[50] To test this hypothesis, we compared $PGE_2$ secretion by Tfh cells primed with either Sup-DCs or TSLP-DCs, and found that Sup-DCs induced higher levels of $PGE_2$ release (Fig. 7f). Then, to evaluate the impact of $PGE_2$ on the secretion of IgG4 and IgE, we cultured B cells with M-CD40L + IL-13 + IL-21 (inducers of both IgG4 and IgE) in the absence or presence of $PGE_2$. Analysis of Ig levels showed that $PGE_2$ significantly impaired IgE secretion but did not significantly affect IgG4 (Fig. 7g and h). Furthermore, IgE secretion was restored following the addition of an EP4 antagonist[51] to the culture medium (Fig. 7h). Overall, these findings suggest that the tumor microenvironment of PDAC favors preferential differentiation/activation of Tfh2 cells with B cell help for all Ig isotypes. Of relevance, Tfh2 cells induce anti-inflammatory IgG4 through IL-13 secretion; whereas these cells inhibit IgE through $PGE_2$ secretion.

## Discussion

The highly immunosuppressive microenvironment has an important role in dictating the dismal prognosis of PDAC. Here, we characterized Tfh cell subsets in three anatomical sites (blood, tumor and TDLN) in PDAC patients and showed that the tumor microenvironment influenced Tfh cell priming and Tfh2 differentiation. Tfh2 cells were highly activated and correlated with worse prognosis in chemo-naïve patients. Mimicking the tumor microenvironment in vitro promoted the differentiation/activation of predominantly Tfh2 cells that induced the production of anti-inflammatory IgG4 Abs by co-cultured B cells. In the same model, a switch to pro-inflammatory IgE was unexpectedly inhibited.

The correlation between high Tfh2 cell frequency within tumors/TDLNs and worse prognosis in chemo-naïve patients contrasts with previous findings regarding Tfh cells in solid tumors, such as breast[52] and colorectal cancer.[53] Consistent with differing behavior in breast and pancreatic cancer, Th1-oriented interferon-γ producing Tfh cells were recently found in active TLS in breast cancer, where they were associated with a lack of recurrence.[54] Meanwhile, consistent with our results, other studies identified $GATA3^+$ Th2 cells in TLS (i.e., bona fide Tfh2 cells) from PDAC[21] and colorectal patients with relapsed disease.[55] These differing findings indicate that factors of the tumor microenvironment potentially have an influence in modulating Tfh cell subset distribution/activation in different tumor types/stages.

In the classical model, anti-tumor immunity develops in the TDLNs.[56] However, antigen-specific T cells can also undergo priming in peripheral tissues, including TLS, where Tfh cells are located.[45] We found Tfh cell clonal expansion in tumor tissue, as well as in the circulation and, to a lower extent, in TDLNs; these findings suggested the potential recognition of tumor antigens, although reactivity to other antigens, such as viral and/or bacterial,[57,58] cannot be excluded. In addition, the presence of Tfh cells sharing identical TCR beta chains within the blood and the other two anatomical sites was consistent with the hypothesis that Tfh cells can be primed in both TDLNs and TLS.

The pro-tumoral role for the Tfh2 cells predominating in our system could be explained by the role of this Tfh subset in promoting anti-inflammatory IgG4 responses, possibly competing with pro-inflammatory IgG1, and in inhibiting pro-inflammatory IgE secretion. Moreover, Tfh2 cells were the only Tfh subset to display high levels of activation in vivo, as indicated by phenotypic and transcriptional analyses. Given the high levels of PD-1 on activated Tfh2 cells, it is tempting to speculate that treatment of PDAC patients with checkpoint inhibitors may even reinforce the negative behavior of pro-tumor Tfh2 cells. This might help to explain the failure of immunotherapy in PDAC. Future experiments will address this important point.

Chemotherapeutic regimens, such as FOLFIRINOX[59,60] and gemcitabine plus nab-paclitaxel,[61] have demonstrated significant survival advantages in both metastatic disease and in the adjuvant setting. Importantly, chemotherapy involves not only direct cytostatic/cytotoxic effects, but also immunomodulatory effects.[62] Here, we found that Tfh2 cell frequency was significantly reduced in patients exhibiting pathological responses to gemcitabine plus nab-paclitaxel. Recently, FOLFIRINOX was shown to increase Th1 cell frequency and decrease Th2 cell frequency in the blood of PDAC patients.[63] In our study, although a trend toward reduced frequencies of highly activated Tfh2 cells was seen in all treated patients, only those receiving gemcitabine plus nab-paclitaxel showed significant effects, indicating that this treatment was more effective than FOLFIRINOX.

Our in vitro mechanistic analyses showed that the tumor microenvironment influenced Ig isotype production by co-cultured B cells. A role for B cells–either anti- or pro-tumor–in tumor immunology is being increasingly recognized.[64] In mouse models of spontaneous pancreatic carcinogenesis, B cells promoted tumor development and progression,[65] while in human disease, $CD20^+$ TILs correlated with either improved[66,67] or reduced survival.[68,69] The functional activities of B cells comprise Ab production, antigen presentation, and the release of cytokines and cytotoxic effector molecules. Abs can have anti- or pro-tumor effects, depending on their isotype. For example, IgG1 and IgE are suggested to contribute to pro-inflammatory anti-tumor immunity, while IgG4 contributes to anti-inflammatory pro-tumor immunity.[64,70–72] Previous studies have shown that high levels of IgG4 in the tumor correlated with reduced patient survival in several solid neoplasms.[73–76] Interestingly, in the case of PDAC, the amount of IgG4 in

intratumor but not those in the peritumor areas correlated with reduced survival.[76] Several mechanisms may account for the tumor-promoting functions of IgG4, such as competition between IgG4 and IgG1 for binding to cancer antigens or to Fc receptors of immune effector cells with reduced functional activity.[64] Our analysis of BCR clonality and SHM showed higher diversity and SHM for *IGHG1*, compared with *IGHG4*, suggesting the presence of a larger number of less expanded, but potentially high-affinity antigen-specific *IGHG1* clones. We may hypothesize cancer-specific IgG1 to be outcompeted on tumor cells by IgG4 that otherwise may be favored by the cytokine milieu in the tumor microenvironment. A novel immune evasion mechanism for non-cancer-specific IgG4 has also been recently reported,[77] whereby IgG4 molecules bind to anti-cancer IgG1 molecules via Fc–Fc interactions. Our finding that IgG1 and IgG4 were partially colocalized within tumor cell nests potentially supports a tumor-promoting role for both cancer-specific and non-cancer-specific IgG4 Abs.

Our in vitro analyses also demonstrated that production of IgE Abs was inhibited despite the presence of the appropriate Th2 cytokines necessary for their secretion; indeed, we found IL-13-dependent secretion of IgG4 but not of IgE. A functional dichotomy between IgG4 and IgE is the basis of the concept of AllergoOncology, whereby opposing strategies should favor expression of tolerogenic IgG4 in allergy and pro-inflammatory IgE in cancer.[78] Thus, in this respect, inhibition of IgE could be regarded as a potential mechanism of immune escape. $PGE_2$ has been reported to exert tumor-promoting functions via several mechanisms including the promotion of tumor growth, invasion, metastasis, and angiogenesis, and the suppression of apoptosis and anti-tumor immunity.[79] The suppression of pro-inflammatory IgE secretion by Tfh2 cell-derived $PGE_2$ suggests a new–and potentially targetable–mechanism for this molecule in promoting cancer progression (Supplementary Figure S9). Interestingly, the results of the first-in-human phase I study with an EP4 receptor antagonist in advanced cancer patients have been recently reported,[80] demonstrating tolerability and immunomodulatory effects.

Future studies for in vivo testing therapeutic strategies targeting the tumor-promoting mechanisms identified here would be worth. To this aim, interestingly, an intratumor Ig distribution reminiscent of the one in PDAC had been reported in the KPC spontaneous murine model of PDAC (i.e., predominance of IgG1 (murine counterpart of human IgG4), and almost no IgE).[81] Though, whether the same mechanisms account for driving induction of IgG1 (i.e., IgG4) and inhibition of IgE in this model still need to be demonstrated.

One limitation of our study is lack of knowledge of the antigens recognized by both Tfh cells and Igs. Indeed, TILs comprise tumor antigen-specific, as well as not tumor antigen-specific immune cells. Nonetheless, our results still proved to be of value, as the Tfh2 cell and IgG4 subsets correlated with worse prognosis in PDAC patients, independently of the antigen recognized.

In conclusion, we have identified tumor-promoting features of Tfh2 and B cell responses in PDAC. Targeting the inflammatory circuits driving Th2 inflammation, for example by inhibition of IL-1 and TSLP, in combination with chemotherapy and/or immunotherapy or possibly re-establishing IgE secretion, should improve overall survival in PDAC.

#### Contributors

LDM and MPP conceived and supervised the study; LDM, FC, ER, and RP designed methodology; FC performed flow cytometry and unsupervised high-dimensional flow cytometry bioinformatic analyses; LDM, FC, and MGC performed experiments, data collection, and data analysis; ER performed TCR-sequencing and data analyses; RP and CB performed bioinformatics and statistical analyses; MSL performed pathology diagnoses and comprising assessment of response to chemotherapy; DL performed RNA-seq experiments; GB, SC, GB, and MF recruited patients, performed surgery, and collected clinical data; CD supervised pathology examination and performed immunohistochemistry; CB supervised TCR-seq analyses; MR recruited patients for neoadjuvant chemotherapy, and collected and discussed clinical data; LDM, FC, ER, RP, CB, and MPP wrote the original draft. LDM, FC, ER, RP, and MPP accessed and verified the data. All authors reviewed and/or edited the final manuscript and were responsible for the decision to submit the manuscript.

#### Data sharing statement

RNA-seq data were deposited to the GEO repository (accession code GSE242917). Other data supporting our findings will be made available by MPP (protti.mariapia@hsr.it) upon reasonable request.

#### Declaration of interests

The authors declare no conflict of interest.

#### Acknowledgements

We wish to thank all patients and their families, as well as Valeria Sordi for advice on the use of and access to the Luminex Instrument, Simona Di Terlizzi and Emanuele Canonico for FACS-sorting, and Lucia Pattarini for helpful suggestions regarding the in vitro studies.

#### Appendix A. Supplementary data

Supplementary data related to this article can be found at https://doi.org/10.1016/j.ebiom.2023.104819.

#### References

1 Hidalgo M. Pancreatic cancer. *N Engl J Med*. 2010;362(17):1605–1617.
2 Rahib L, Smith BD, Aizenberg R, et al. Projecting cancer incidence and deaths to 2030: the unexpected burden of thyroid, liver, and pancreas cancers in the United States. *Cancer Res*. 2014;74(11):2913–2921.
3 Leinwand J, Miller G. Regulation and modulation of antitumor immunity in pancreatic cancer. *Nat Immunol*. 2020;21(10):1152–1159.
4 Tassi E, Gavazzi F, Albarello L, et al. Carcinoembryonic antigen-specific but not antiviral $CD4^+$ T cell immunity is impaired in pancreatic carcinoma patients. *J Immunol*. 2008;181(9):6595–6603.
5 De Monte L, Reni M, Tassi E, et al. Intratumor T helper type 2 cell infiltrate correlates with cancer-associated fibroblast thymic stromal lymphopoietin production and reduced survival in pancreatic cancer. *J Exp Med*. 2011;208(3):469–478.

6 Protti MP, De Monte L. Cross-talk within the tumor microenvironment mediates Th2-type inflammation in pancreatic cancer. *OncoImmunology*. 2012;1(1):89–91.
7 De Monte L, Woermann S, Brunetto E, et al. Basophil recruitment into tumor draining lymph nodes correlates with Th2 inflammation and reduced survival in pancreatic cancer patients. *Cancer Res*. 2016;76:1792–1803.
8 Brunetto E, De Monte L, Balzano G, et al. The IL-1/IL-1 receptor axis and tumor cell released inflammasome adaptor ASC are key regulators of TSLP secretion by cancer associated fibroblasts in pancreatic cancer. *J Immunother Cancer*. 2019;7(1):45.
9 Wormann SM, Song L, Ai J, et al. Loss of P53 function activates JAK2-STAT3 signaling to promote pancreatic tumor growth, stroma modification, and gemcitabine resistance in mice and is associated with patient survival. *Gastroenterology*. 2016;151(1):180–193.e112.
10 Ochi A, Nguyen AH, Bedrosian AS, et al. MyD88 inhibition amplifies dendritic cell capacity to promote pancreatic carcinogenesis via Th2 cells. *J Exp Med*. 2012;209(9):1671–1687.
11 Kurahara H, Shinchi H, Mataki Y, et al. Significance of M2-polarized tumor-associated macrophage in pancreatic cancer. *J Surg Res*. 2011;167(2):e211–e219.
12 Piro G, Simionato F, Carbone C, et al. A circulating TH2 cytokines profile predicts survival in patients with resectable pancreatic adenocarcinoma. *OncoImmunology*. 2017;6(9):e1322242.
13 Dey P, Li J, Zhang J, et al. Oncogenic KRAS-driven metabolic reprogramming in pancreatic cancer cells utilizes cytokines from the tumor microenvironment. *Cancer Discov*. 2020;10(4):608–625.
14 Gunderson AJ, Kaneda MM, Tsujikawa T, et al. Bruton tyrosine kinase-dependent immune cell cross-talk drives pancreas cancer. *Cancer Discov*. 2016;6(3):270–285.
15 Nizri E, Bar-David S, Aizic A, et al. Desmoplasia in lymph node metastasis of pancreatic adenocarcinoma reveals activation of cancer-associated fibroblasts pattern and T-helper 2 immune cell infiltration. *Pancreas*. 2019;48(3):367–373.
16 Di Caro G, Cortese N, Castino GF, et al. Dual prognostic significance of tumour-associated macrophages in human pancreatic adenocarcinoma treated or untreated with chemotherapy. *Gut*. 2016;65(10):1710–1720.
17 Alam A, Levanduski E, Denz P, et al. Fungal mycobiome drives IL-33 secretion and type 2 immunity in pancreatic cancer. *Cancer Cell*. 2022;40(2):153–167.e11.
18 Kurahara H, Takao S, Maemura K, et al. M2-polarized tumor-associated macrophage infiltration of regional lymph nodes is associated with nodal lymphangiogenesis and occult nodal involvement in pN0 pancreatic cancer. *Pancreas*. 2013;42(1):155–159.
19 Hiraoka N, Ino Y, Yamazaki-Itoh R, et al. Intratumoral tertiary lymphoid organ is a favourable prognosticator in patients with pancreatic cancer. *Br J Cancer*. 2015;112(11):1782–1790.
20 Gunderson AJ, Rajamanickam V, Bui C, et al. Germinal center reactions in tertiary lymphoid structures associate with neoantigen burden, humoral immunity and long-term survivorship in pancreatic cancer. *OncoImmunology*. 2021;10(1):1900635.
21 Liudahl SM, Betts CB, Sivagnanam S, et al. Leukocyte heterogeneity in pancreatic ductal adenocarcinoma: phenotypic and spatial features associated with clinical outcome. *Cancer Discov*. 2021;11(8):2014–2031.
22 Delvecchio FR, Fincham REA, Spear S, et al. Pancreatic cancer chemotherapy is potentiated by induction of tertiary lymphoid structures in mice. *Cell Mol Gastroenterol Hepatol*. 2021;12(5):1543–1565.
23 Ahmed A, Kohler S, Klotz R, et al. Tertiary lymphoid structures and their association to immune phenotypes and circulatory IL2 levels in pancreatic ductal adenocarcinoma. *OncoImmunology*. 2022;11(1):2027148.
24 Fridman WH, Meylan M, Petitprez F, et al. B cells and tertiary lymphoid structures as determinants of tumour immune contexture and clinical outcome. *Nat Rev Clin Oncol*. 2022;19:441–457.
25 Vinuesa CG, Linterman MA, Yu D, et al. Follicular helper T Cells. *Annu Rev Immunol*. 2016;34:335–368.
26 Crotty S. T Follicular helper cell biology: a decade of discovery and diseases. *Immunity*. 2019;50(5):1132–1148.
27 Gutierrez-Melo N, Baumjohann D. T follicular helper cells in cancer. *Trends Cancer*. 2023;9(4):309–325.
28 Morita R, Schmitt N, Bentebibel SE, et al. Human blood CXCR5(+) CD4(+) T cells are counterparts of T follicular cells and contain specific subsets that differentially support antibody secretion. *Immunity*. 2011;34(1):108–121.
29 Perfetto SP, Ambrozak D, Nguyen R, et al. Quality assurance for polychromatic flow cytometry using a suite of calibration beads. *Nat Protoc*. 2012;7(12):2067–2079.
30 Nowicka M, Krieg C, Crowell HL, et al. CyTOF workflow: differential discovery in high-throughput high-dimensional cytometry datasets. *F1000Res*. 2017;6:748.
31 Moschetti G, Vasco C, Clemente F, et al. Deep phenotyping of T-cells derived from the aneurysm wall in a pediatric case of subarachnoid hemorrhage. *Front Immunol*. 2022;13:866558.
32 Bolotin DA, Mamedov IZ, Britanova OV, et al. Next generation sequencing for TCR repertoire profiling: platform-specific features and correction algorithms. *Eur J Immunol*. 2012;42(11):3073–3083.
33 Ruggiero E, Nicolay JP, Fronza R, et al. High-resolution analysis of the human T-cell receptor repertoire. *Nat Commun*. 2015;6:8081.
34 Bolotin DA, Poslavsky S, Mitrophanov I, et al. MiXCR: software for comprehensive adaptive immunity profiling. *Nat Methods*. 2015;12(5):380–381.
35 Balestrieri C, Alfarano G, Milan M, et al. Co-optation of tandem DNA repeats for the maintenance of mesenchymal identity. *Cell*. 2018;173(5):1150–1164.e14.
36 Dobin A, Davis CA, Schlesinger F, et al. STAR: ultrafast universal RNA-seq aligner. *Bioinformatics*. 2013;29(1):15–21.
37 Liao Y, Smyth GK, Shi W. featureCounts: an efficient general purpose program for assigning sequence reads to genomic features. *Bioinformatics*. 2014;30(7):923–930.
38 Love MI, Huber W, Anders S. Moderated estimation of fold change and dispersion for RNA-seq data with DESeq2. *Genome Biol*. 2014;15(12):550.
39 Langfelder P, Horvath S. WGCNA: an R package for weighted correlation network analysis. *BMC Bioinformatics*. 2008;9:559.
40 Gu Z, Eils R, Schlesner M. Complex heatmaps reveal patterns and correlations in multidimensional genomic data. *Bioinformatics*. 2016;32(18):2847–2849.
41 Chen EY, Tan CM, Kou Y, et al. Enrichr: interactive and collaborative HTML5 gene list enrichment analysis tool. *BMC Bioinformatics*. 2013;14:128.
42 Eden E, Navon R, Steinfeld I, et al. GOrilla: a tool for discovery and visualization of enriched GO terms in ranked gene lists. *BMC Bioinformatics*. 2009;10:48.
43 Supek F, Bosnjak M, Skunca N, et al. REVIGO summarizes and visualizes long lists of gene ontology terms. *PLoS One*. 2011;6(7):e21800.
44 Song L, Cohen D, Ouyang Z, et al. TRUST4: immune repertoire reconstruction from bulk and single-cell RNA-seq data. *Nat Methods*. 2021;18(6):627–630.
45 Dieu-Nosjean MC, Giraldo NA, Kaplon H, et al. Tertiary lymphoid structures, drivers of the anti-tumor responses in human cancers. *Immunol Rev*. 2016;271(1):260–275.
46 Hartman DJ, Krasinskas AM. Assessing treatment effect in pancreatic cancer. *Arch Pathol Lab Med*. 2012;136(1):100–109.
47 Pattarini L, Trichot C, Bogiatzi S, et al. TSLP-activated dendritic cells induce human T follicular helper cell differentiation through OX40-ligand. *J Exp Med*. 2017;214(5):1529–1546.
48 Jensen-Jarolim E, Turner MC, Karagiannis SN. AllergoOncology: IgE- and IgG4-mediated immune mechanisms linking allergy with cancer and their translational implications. *J Allergy Clin Immunol*. 2017;140(4):982–984.
49 Oyesola OO, Tait Wojno ED. Prostaglandin regulation of type 2 inflammation: from basic biology to therapeutic interventions. *Eur J Immunol*. 2021;51(10):2399–2416.
50 Garrone P, Galibert L, Rousset F, et al. Regulatory effects of prostaglandin E2 on the growth and differentiation of human B lymphocytes activated through their CD40 antigen. *J Immunol*. 1994;152(9):4282–4290.
51 Wu J, Wang Y, Zhou Y, et al. PPARg as an E3 ubiquitin-ligase impedes phosphate-Stat6 stability and promotes prostaglandins E2-mediated Inhibition of IgE production in asthma. *Front Immunol*. 2020;11:1224.
52 Gu-Trantien C, Loi S, Garaud S, et al. CD4(+) follicular helper T cell infiltration predicts breast cancer survival. *J Clin Invest*. 2013;123(7):2873–2892.
53 Bindea G, Mlecnik B, Tosolini M, et al. Spatiotemporal dynamics of intratumoral immune cells reveal the immune landscape in human cancer. *Immunity*. 2013;39(4):782–795.
54 Noel G, Fontsa ML, Garaud S, et al. Functional Th1-oriented T follicular helper cells that infiltrate human breast cancer promote effective adaptive immunity. *J Clin Invest*. 2021;131(19):e139905.

55 Yamaguchi K, Ito M, Ohmura H, et al. Helper T cell-dominant tertiary lymphoid structures are associated with disease relapse of advanced colorectal cancer. *OncoImmunology*. 2020;9(1):1724763.
56 Chen DS, Mellman I. Oncology meets immunology: the cancer-immunity cycle. *Immunity*. 2013;39(1):1–10.
57 Meng Q, Valentini D, Rao M, et al. CMV and EBV targets recognized by tumor-infiltrating B lymphocytes in pancreatic cancer and brain tumors. *Sci Rep*. 2018;8(1):17079.
58 Overacre-Delgoffe AE, Bumgarner HJ, Cillo AR, et al. Microbiota-specific T follicular helper cells drive tertiary lymphoid structures and anti-tumor immunity against colorectal cancer. *Immunity*. 2021;54(12):2812–2824.e4.
59 Conroy T, Desseigne F, Ychou M, et al. FOLFIRINOX versus gemcitabine for metastatic pancreatic cancer. *N Engl J Med*. 2011;364(19):1817–1825.
60 Conroy T, Hammel P, Hebbar M, et al. FOLFIRINOX or gemcitabine as adjuvant therapy for pancreatic cancer. *N Engl J Med*. 2018;379(25):2395–2406.
61 Von Hoff DD, Ervin T, Arena FP, et al. Increased survival in pancreatic cancer with nab-paclitaxel plus gemcitabine. *N Engl J Med*. 2013;369(18):1691–1703.
62 Galluzzi L, Humeau J, Buque A, et al. Immunostimulation with chemotherapy in the era of immune checkpoint inhibitors. *Nat Rev Clin Oncol*. 2020;17(12):725–741.
63 Peng H, James CA, Cullinan DR, et al. Neoadjuvant FOLFIRINOX therapy is associated with increased effector T cells and reduced suppressor cells in patients with pancreatic cancer. *Clin Cancer Res*. 2021;27(24):6761–6771.
64 Shalapour S, Karin M. The neglected brothers come of age: B cells and cancer. *Semin Immunol*. 2021;52:101479.
65 Minici C, Testoni S, Della-Torre E. B-lymphocytes in the pathophysiology of pancreatic adenocarcinoma. *Front Immunol*. 2022;13:867902.
66 Castino GF, Cortese N, Capretti G, et al. Spatial distribution of B cells predicts prognosis in human pancreatic adenocarcinoma. *OncoImmunology*. 2016;5(4):e1085147.
67 Tewari N, Zaitoun AM, Arora A, et al. The presence of tumour-associated lymphocytes confers a good prognosis in pancreatic ductal adenocarcinoma: an immunohistochemical study of tissue microarrays. *BMC Cancer*. 2013;13:436.
68 Wang WQ, Liu L, Xu HX, et al. Infiltrating immune cells and gene mutations in pancreatic ductal adenocarcinoma. *Br J Surg*. 2016;103(9):1189–1199.
69 Takahashi R, Macchini M, Sunagawa M, et al. Interleukin-1beta-induced pancreatitis promotes pancreatic ductal adenocarcinoma via B lymphocyte-mediated immune suppression. *Gut*. 2021;70(2):330–341.
70 Sharonov GV, Serebrovskaya EO, Yuzhakova DV, et al. B cells, plasma cells and antibody repertoires in the tumour microenvironment. *Nat Rev Immunol*. 2020;20(5):294–307.
71 Karagiannis S, Nestle F, Gould H. *IgE interacts with potent effector cells against tumors: ADCC and ADCP*. Humana Press Inc; 2010:185–213 Chapter in Book.
72 Crescioli S, Correa I, Karagiannis P, et al. IgG4 characteristics and functions in cancer immunity. *Curr Allergy Asthma Rep*. 2016;16(1):7.
73 Kimura Y, Harada K, Nakanuma Y. Pathologic significance of immunoglobulin G4-positive plasma cells in extrahepatic cholangiocarcinoma. *Hum Pathol*. 2012;43(12):2149–2156.
74 Miyatani K, Saito H, Murakami Y, et al. A high number of IgG4-positive cells in gastric cancer tissue is associated with tumor progression and poor prognosis. *Virchows Arch*. 2016;468(5):549–557.
75 Toney NJ, Opdenaker LM, Cicek K, et al. Tumor-B-cell interactions promote isotype switching to an immunosuppressive IgG4 antibody response through upregulation of IL-10 in triple negative breast cancers. *J Transl Med*. 2022;20(1):112.
76 Liu Q, Niu Z, Li Y, et al. Immunoglobulin G4 (IgG4)-positive plasma cell infiltration is associated with the clinicopathologic traits and prognosis of pancreatic cancer after curative resection. *Cancer Immunol Immunother*. 2016;65(8):931–940.
77 Wang H, Xu Q, Zhao C, et al. An immune evasion mechanism with IgG4 playing an essential role in cancer and implication for immunotherapy. *J Immunother Cancer*. 2020;8(2):e000661.
78 Jensen-Jarolim E, Bax HJ, Bianchini R, et al. AllergoOncology: opposite outcomes of immune tolerance in allergy and cancer. *Allergy*. 2018;73(2):328–340.
79 Finetti F, Travelli C, Ercoli J, et al. Prostaglandin E2 and cancer: insight into tumor progression and immunity. *Biology*. 2020;9(12):434.
80 Hong DS, Parikh A, Shapiro GI, et al. First-in-human phase I study of immunomodulatory E7046, an antagonist of PGE(2)-receptor E-type 4 (EP4), in patients with advanced cancers. *J Immunother Cancer*. 2020;8(1):e000222.
81 Spear S, Candido JB, McDermott JR, et al. Discrepancies in the tumor microenvironment of spontaneous and orthotopic murine models of pancreatic cancer uncover a new immunostimulatory phenotype for B cells. *Front Immunol*. 2019;10:542.